J. Fluid Mech. (2008), *vol.* 614, *pp.* 145–172. © 2008 Cambridge University Press
doi:10.1017/S0022112008003364 Printed in the United Kingdom

The piecewise constant symmetric potential vorticity vortex in geophysical flows

ÁLVARO VIÚDEZ
Institut de Ciències del Mar, CSIC, 08003 Barcelona, Spain

(Received 10 January 2008 and in revised form 5 July 2008)

The concept of piecewise constant symmetric vortex in the context of three-dimensional baroclinic balanced geophysical flows is explored. The pressure gradients generated by horizontal cylinders and spherical balls of uniform potential vorticity (PV), or uniform material invariants, are obtained either analytically or numerically, in the general case of Boussinesq and f-plane dynamics as well as under the quasi-geostrophic and semigeostrophic dynamical approximations. Based on the order of magnitude of the different terms in the PV inversion equation, approximated PV equations are deduced. In some of these cases, radial solutions are possible and the interior and exterior solutions are found analytically. In the case of non-radial dependence, exterior solutions can be found numerically. Linear, and upper and lower bound approximations to the full PV inversion equations, and their respective solutions, are also included. However, the general solution for the pressure gradient in the vortex exterior does not have spherical symmetry and remains as an important theoretical challenge. It is suggested that, in order to maintain everywhere the inertial and static stability of the balanced geophysical flows, small balls of finite radius, rather than PV singularities, could become, specially in numerical applications, useful mathematical objects.

1. Introduction

The point vortex, as well as similar point singularities such as the point electric charge and the point mass, is a simple but important theoretical model, useful in understanding the behaviour of complex flows. The paradigm of a point vortex occurs in two-dimensional flows of incompressible inviscid fluids, where the vorticity is the relevant materially conserved quantity. Vortex multipoles may be considered, in this case, as point singularities in the vorticity distribution (e.g. Lamb 1932; Batchelor 1967; Saffman 1992; Voropayev & Afanasyev 1994). In the case of three-dimensional rotating and stratified fluids, such as those in the ocean and atmosphere, the relevant scalar quantity is the Beltrami–Rossby–Ertel potential vorticity (PV), which is materially conserved when the flow is adiabatic and inviscid (Beltrami 1871; Rossby 1940; Ertel 1942; Kurgansky & Tatarskaya 1987; Müller 1995; Viúdez 2001). This material conservation and the fact that PV is unaffected by inertia–gravity waves make PV an excellent physical quantity for investigating balanced (void of waves) mesoscale and synoptic scale mid-latitude geophysical systems, where the flow is both inertially and statically stable. The purpose of this paper is to investigate the feasibility and utility of point singularities in the PV distribution in the dynamics of these balanced geophysical flows.

https://doi.org/10.1017/S0022112008003364 Published online by Cambridge University Press

After a first look at the problem of defining the point PV vortex in balanced geophysical flows, it becomes clear that this task is not merely a straightforward application to baroclinic flows of the point concept used to define the point electric charge, point gravity mass or point vortex in two-dimensional flows. The main difficulty is that when the volume of a ball of PV is reduced while the PV density is increased in such a way that the amount of PV inside the ball is kept constant, the flow becomes inertially and statically unstable in the exterior vicinity of the PV ball. When this happens, the flow departs from the balance regime in which PV is most useful, since the PV singularities themselves would become a source of inertia–gravity waves. This difficulty is circumvented here by abandoning the concept of point PV vortex and introducing the concept of a small piecewise constant symmetric PV vortex, or simply a PV ball, spherical in the quasi-geostrophic space, having a small radius relative to the larger spatial scales of interest. For example, in numerical applications, the PV ball radius could be smaller than the numerical grid size.

The basic dynamics and definitions of the relevant quantities are first briefly introduced in § 2. The instability problems appearing in the definition of PV singularities are then made precise in the case of a rectilinear horizontal PV cylinder (§ 3). In this case, the geostrophic flow is an exact solution of the dynamical equations, and an analytical solution of the pressure gradient in terms of the PV anomaly is possible. The full nonlinear PV inversion equation in terms of the pressure is introduced (§ 4), and the interior pressure solution for the PV ball is obtained, whereas the exterior solution is found numerically. The same PV ball concept is next investigated within the quasi-geostrophic (QG, § 5) and semi-geostrophic (SG, § 6) approximations, in which interior and exterior radial pressure solutions (i.e. with spherical symmetry) are possible. These QG and SG radial solutions are already known (Thorpe & Bishop 1994, 1995) and are included here for completeness and to stress that the difficulty in finding a general exact solution is caused by its non-radial property. The common variable used to compare these different dynamics is their respective material invariants (the QG and SG material invariants), as well as the PV of these flows. Based on the order of magnitude of the different terms in the PV inversion equation, approximated PV equations are deduced (§ 7). In some of these cases radial solutions are possible and the interior and exterior solutions are found analytically. In the case of non-radial dependence, exterior solutions can be found numerically. Linear, and upper and lower bound approximations to the full PV inversion equations, and their respective solutions, are also included. Concluding remarks are given (§ 8).

2. Basic dynamics and PV

We consider the isochoric (volume-preserving) motion of a stable stratified fluid, under the Boussinesq approximation, in a reference frame rotating with constant angular velocity $f/2$ around the vertical z-axis with respect to an inertial frame (the f-plane approximation typical of mesoscale and synoptic scale dynamics). Here, f is the vertical component of the planetary vorticity (or Coriolis parameter). It is convenient to introduce the density anomaly ρ' defined as

$$\rho'(\boldsymbol{x}, t) \equiv \rho(\boldsymbol{x}, t) - \varrho_0 z - \rho_0, \tag{2.1}$$

where $\boldsymbol{x} = (x, y, z)$, ρ is the mass density, and $\rho_0 > 0$ and $\varrho_0 < 0$ are given constants that need not be specified under the Boussinesq approximation. We introduce the pressure anomaly $\mathscr{P}$ as the pressure p, plus a term $f^2(x^2 + y^2)/(8\rho_0)$ due to the

https://doi.org/10.1017/S0022112008003364 Published online by Cambridge University Press

planetary centripetal potential $-f^2(x^2+y^2)/8$, minus the hydrostatic pressure due to a constant vertical density stratification

$$\mathscr{P}(\boldsymbol{x},t) \equiv p(\boldsymbol{x},t) + f^2(x^2+y^2)/(8\rho_0) + g\left(\rho_0 + \tfrac{1}{2}\varrho_0 z\right) z, \tag{2.2}$$

where g is the acceleration due to gravity. The Boussinesq approximation in the vertical component of the momentum equation is therefore

$$-\frac{1}{\rho}\left(p_z + g\rho\right) \cong -\alpha_0\left(p_z + g\rho\right) = -\alpha_0 \mathscr{P}_z - \alpha_0 g\rho', \tag{2.3}$$

where $\alpha_0 \equiv \rho_0^{-1}$ is a constant specific volume, and the subscript z means the partial derivative with respect to z. Vector components here always refer to Cartesian components. The basic equations are the non-hydrostatic balance of linear momentum in a rotating frame under the f-plane and Boussinesq approximations, the mass conservation equation, and the isochoric condition,

$$\frac{\mathrm{d}\boldsymbol{u}_h}{\mathrm{d}t} + f\hat{\boldsymbol{k}} \times \boldsymbol{u}_h = -\alpha_0 \nabla_h \mathscr{P}, \tag{2.4a}$$

$$\frac{\mathrm{d}w}{\mathrm{d}t} = -\alpha_0 \frac{\partial \mathscr{P}}{\partial z} - \alpha_0 g\rho', \tag{2.4b}$$

$$\frac{\mathrm{d}\rho}{\mathrm{d}t} + \rho\, \nabla \cdot \boldsymbol{u} = 0, \tag{2.4c}$$

$$\nabla \cdot \boldsymbol{u} = 0. \tag{2.4d}$$

As usual, symbol $\mathrm{d}(\ )/\mathrm{d}t \equiv \partial(\ )/\partial t + \boldsymbol{u}\cdot\nabla(\ )$ denotes the material time derivative in the rotating reference frame, and $\hat{\boldsymbol{k}}$ is the vertical unit vector. The unknowns are the three-dimensional velocity field $\boldsymbol{u} = (u, v, w)$, the pressure anomaly $\mathscr{P}$, and the density anomaly ρ'.

It is convenient to express ρ in terms of the field d defined by

$$d \equiv (\rho - \rho_0)/\varrho_0. \tag{2.5}$$

The value $d(\boldsymbol{x},t)$ represents the depth, or vertical location, that the isopycnal located at $\boldsymbol{x}$ at time t has in the reference density configuration defined by $\rho_0 + \varrho_0 z$. Thus, the density field is expressed in terms of distances. The displacement $\mathscr{D}$ of isopycnals with respect to the reference density configuration is defined as

$$\mathscr{D}(\boldsymbol{x},t) \equiv z - d(\boldsymbol{x},t). \tag{2.6}$$

The value $\mathscr{D}(\boldsymbol{x},t)$ is the vertical displacement of the isopycnal currently located at $(\boldsymbol{x},t)$ with respect to its reference position. The incompressibility condition $\mathrm{d}\rho/\mathrm{d}t = \mathrm{d}d/\mathrm{d}t = 0$ is expressed in terms of $\mathscr{D}$ as

$$\frac{\mathrm{d}\mathscr{D}}{\mathrm{d}t} = w. \tag{2.7}$$

The vertical displacement of isopycnals $\mathscr{D}$ is related to ρ and ρ' by

$$N^2(\mathscr{D}(\boldsymbol{x},t) - z) = g\left(\alpha_0\rho(\boldsymbol{x},t) - 1\right), \quad \mathscr{D} = -\frac{\rho'}{\varrho_0}, \tag{2.8}$$

where $N^2 \equiv -\alpha_0\, g\varrho_0$ is the square of the constant background Brunt–Väisälä frequency. Thus, the buoyancy term $\alpha_0 g\rho'$ in (2.4b) can be replaced with $N^2\mathscr{D}$. We note that static instability ($\partial\rho/\partial z > 0$) occurs when the stratification number $\partial\mathscr{D}/\partial z > 1$.

https://doi.org/10.1017/S0022112008003364 Published online by Cambridge University Press

For any quantity χ, let $\tilde{\chi} \equiv \chi/f$. The geostrophic velocity shear is defined through the thermal wind expression

$$\tilde{\boldsymbol{u}}_z^g \equiv -c^2 \hat{\boldsymbol{k}} \times \nabla_h \mathscr{D}, \tag{2.9}$$

where the background Prandtl ratio $c = \epsilon^{-1} \equiv N/f$. Using (2.7), it follows that the rate of change of $\nabla\mathscr{D}$ is

$$\frac{\mathrm{d}}{\mathrm{d}t}\nabla\mathscr{D} = \nabla w - \nabla \boldsymbol{u} \cdot \nabla\mathscr{D}. \tag{2.10}$$

The vorticity equation consistent with (2.4) is

$$\frac{\mathrm{d}\tilde{\boldsymbol{\omega}}}{\mathrm{d}t} = \tilde{\boldsymbol{\omega}} \cdot \nabla \boldsymbol{u} + \boldsymbol{u}_z + f c^2 \hat{\boldsymbol{k}} \times \nabla_h \mathscr{D}, \tag{2.11}$$

where the relative vorticity $\boldsymbol{\omega} \equiv \nabla \times \boldsymbol{u} = (\zeta, \xi, \eta)$. The rates of change of $\nabla\mathscr{D}$ (2.10) and $\boldsymbol{\omega}$ (2.11) imply the material conservation of PV

$$\frac{\mathrm{d}\varpi}{\mathrm{d}t} = 0, \tag{2.12}$$

where

$$\varpi \equiv \Pi - 1 \equiv (\tilde{\boldsymbol{\omega}} + f\hat{\boldsymbol{k}}) \cdot \nabla d - 1 = \tilde{\zeta} - \mathscr{D}_z - \tilde{\boldsymbol{\omega}} \cdot \nabla\mathscr{D} \tag{2.13}$$

is the dimensionless PV density anomaly. Since the flow is isochoric, both PV density (Π) and specific PV (Π/ρ) are materially conserved. If the spatial distribution of the PV anomaly $\varpi(\boldsymbol{x})$ is known, and considering the vorticity $\tilde{\boldsymbol{\omega}}(\mathscr{P}(\boldsymbol{x}))$ and the vertical displacement $\mathscr{D}(\mathscr{P}(\boldsymbol{x}))$ as functions of the spatial derivatives of the unknown pressure anomaly $\mathscr{P}$, the PV definition (2.13) becomes an equation for $\mathscr{P}(\boldsymbol{x})$. This is called the PV inversion problem, and is the major problem addressed in this paper in the particular case of radial and homogeneous distributions of PV.

3. The straight line PV vortex

We consider first the simple steady straight shear flow because exact solutions of the dynamical equations (2.4) can be obtained in this case, and this helps to understand the characteristics of the PV ball in three dimensions. We consider straight horizontal flow ($u = w = 0$) constant along the y-axis, so that the flow variables ($v, \mathscr{D}, \mathscr{P}$) depend only on x and z. The flow is steady, in geostrophic balance, and hydrostatic. The basic equations (2.4) reduce to

$$\tilde{v} = \Phi_x, \tag{3.1a}$$

$$-c^2\mathscr{D} = \Phi_z, \tag{3.1b}$$

where, to simplify the notation, we define the scaled pressure anomaly

$$\Phi(x, z) \equiv \frac{\alpha_0}{f^2}\mathscr{P}(x, z). \tag{3.2}$$

It is also mathematically convenient to introduce the z-coordinate vertically stretched by the background Prandtl ratio $\hat{z} \equiv cz$, which defines the QG space $(x, \hat{z})$. The vertical vorticity, stratification anomaly, and the nonlinear terms in the definition of PV (2.13) are

$$\tilde{\zeta} = \tilde{v}_x = \Phi_{xx}, \tag{3.3a}$$

$$\mathscr{D}_z = -\epsilon^2\Phi_{zz} = -\Phi_{\hat{z}\hat{z}}, \tag{3.3b}$$

$$\tilde{\boldsymbol{\omega}} \cdot \nabla\mathscr{D} = -\tilde{v}_z\mathscr{D}_x + \tilde{v}_x\mathscr{D}_z = -\Phi_{xx}\Phi_{\hat{z}\hat{z}} + \Phi_{x\hat{z}}^2. \tag{3.3c}$$

https://doi.org/10.1017/S0022112008003364 Published online by Cambridge University Press

This results in the relation between PV anomaly and pressure anomaly,

$$\varpi = \hat{\nabla}^2\Phi + \begin{vmatrix} \Phi_{xx} & \Phi_{\hat{z}x} \\ \Phi_{x\hat{z}} & \Phi_{\hat{z}\hat{z}} \end{vmatrix} = \hat{\nabla}^2\Phi + \hat{\mathrm{H}}\{\Phi\}, \tag{3.4}$$

where $\hat{\nabla}^2 \equiv \partial^2/\partial x^2 + \partial^2/\partial \hat{z}^2$ and $\hat{\mathrm{H}} \equiv \det \hat{\nabla}\hat{\nabla}$ are the Laplacian and the Hessian operators, respectively, in the $(x, \hat{z})$-space. The PV inversion equation above can be further simplified by introducing the new potential

$$\Psi \equiv \Phi + \tfrac{1}{2}r^2, \tag{3.5}$$

where the position vector $\boldsymbol{r}(x, \hat{z}) \equiv x\hat{\boldsymbol{\imath}} + \hat{z}\hat{\boldsymbol{k}}$ and $r(x, \hat{z}) = \sqrt{x^2 + \hat{z}^2}$. The potential Ψ satisfies a Monge–Ampère equation,

$$\Pi = \hat{\mathrm{H}}\{\Psi\}. \tag{3.6}$$

For radial PV distributions in the $(x, \hat{z})$-space $\Pi(r) = \varpi(r) + 1$, we assume radial solutions $\Psi(r)$, so that (3.6) becomes

$$\Pi = \frac{\Psi_r \Psi_{rr}}{r} \quad \Rightarrow \quad 2r\Pi = \left(\Psi_r^2\right)_r. \tag{3.7}$$

A first spatial integration of (3.7) from $r' = 0$ to $r' = r$ yields

$$2\int_0^r r'\varpi(r')\,\mathrm{d}r' + r^2 = \Psi_r^2(r), \tag{3.8}$$

where we have taken $\Psi_r(0) = 0$ consistently with a finite Π and $\Psi_{rr} \neq 0$ at $r = 0$ in (3.7).

We now specify that the radial PV anomaly distribution is everywhere zero except inside a horizontal cylinder, limited by a circle of radius r_0 and centred at the origin of the $(x, \hat{z})$-plane, where it has a constant value ϖ_0,

$$\varpi(r) = \begin{cases} \varpi_0, & r \leqslant r_0, \\ 0, & r > r_0. \end{cases} \tag{3.9}$$

With this PV anomaly distribution, the integral relation (3.8) provides the interior (Ψ_{ir}) and exterior (Ψ_{er}) solutions of Ψ_r,

$$\Psi_r(r) = \begin{cases} \Psi_{ir}(r) = r\sqrt{\Pi_0}, & r \leqslant r_0, \\ \Psi_{er}(r) = \sqrt{r^2 + \varpi_0 r_0^2}, & r > r_0, \end{cases} \tag{3.10}$$

where $\Pi_0 \equiv 1 + \varpi_0$ is the total PV density inside the PV cylinder. The positive root has been taken in (3.10) as a consequence of imposing inertial stability ($\tilde{\zeta} > -1$ in the case of negative vorticity shear; see e.g. Holton 2004, p. 205) and static stability (stratification anomaly $\mathscr{D}_z < 1$) inside the PV cylinder($r \leqslant r_0$), that is

$$\left.\begin{aligned} \tilde{\zeta} = \Phi_{xx} = \pm\sqrt{\Pi_0} - 1 \quad &> \quad -1 \\ \mathscr{D}_z = -\Phi_{\hat{z}\hat{z}} = -(\pm\sqrt{\Pi_0} - 1) \quad &< \quad 1 \end{aligned}\right\} \Rightarrow \Psi_{ir}(r) = +r\sqrt{\Pi_0}. \tag{3.11}$$

The potential gradient Ψ_r is continuous at $r = r_0$ where $\Psi_{ir}(r_0) = \Psi_{er}(r_0) = r_0\sqrt{\Pi_0}$.

From (3.5) and (3.10) the gradient of $\Phi(r)$ is

$$\Phi_r(r) = \Psi_r(r) - r = \begin{cases} \Phi_{ri}(r) = r(\sqrt{\Pi_0} - 1), & r \leqslant r_0, \\ \Phi_{re}(r) = \sqrt{r^2 + \varpi_0 r_0^2} - r, & r > r_0. \end{cases} \tag{3.12}$$

In the limit $r \to \infty$, the external gradient $\Phi_{re}(r)$ tends to 0 as $\varpi_0 r_0^2/r$.

https://doi.org/10.1017/S0022112008003364 Published online by Cambridge University Press

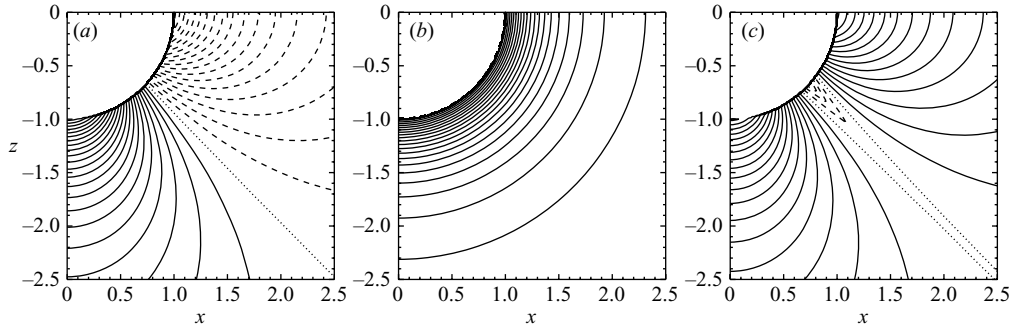


FIGURE 1. Distributions in the $(x, \hat{z})$-plane of (a) the vertical vorticity $\tilde{\zeta}$ (contour interval $\Delta = 10^{-2}$), (b) the nonlinear term $\tilde{\boldsymbol{\omega}} \cdot \nabla \mathscr{D}$ ($\Delta = 2 \times 10^{-3}$), and (c) the difference $|\tilde{\zeta}| - |\tilde{\boldsymbol{\omega}} \cdot \nabla \mathscr{D}|$ ($\Delta = 10^{-2}$). The cylinder radius $r_0 = 1$ and PV anomaly $\varpi_0 = 0.5$. In this and subsequent similar figures, solid contour lines indicate positive values, dashed lines negative, and the dotted line is the zero contour.

Thus, the linear terms contributing to the PV anomaly are

$$\tilde{\zeta} = \begin{cases} \sqrt{\Pi_0} - 1, & r \leqslant r_0, \\ \dfrac{r^4 + \varpi_0 r_0^2 \hat{z}^2}{r^3 \sqrt{r^2 + \varpi_0 r_0^2}} - 1, & r > r_0, \end{cases} \qquad \mathscr{D}_z = \begin{cases} 1 - \sqrt{\Pi_0}, & r \leqslant r_0, \\ 1 - \dfrac{r^4 + \varpi_0 r_0^2 x^2}{r^3 \sqrt{r^2 + \varpi_0 r_0^2}}, & r > r_0. \end{cases} \tag{3.13}$$

The flow is therefore everywhere statically stable ($\mathscr{D}_z < 1$) as long as $\Pi_0 > 0$. The nonlinear term in the definition of the PV anomaly (3.3c) is

$$\tilde{\boldsymbol{\omega}} \cdot \nabla \mathscr{D} = \begin{cases} -\Pi_0 + 2\sqrt{\Pi_0} - 1, & r \leqslant r_0, \\ \dfrac{2r^2 + \varpi_0 r_0^2}{r \sqrt{r^2 + \varpi_0 r_0^2}} - 2, & r > r_0. \end{cases} \tag{3.14}$$

The vertical vorticity $\tilde{\zeta}(x, \hat{z})$ is shown in figure 1(a) for a moderate positive PV anomaly $\varpi_0 = 0.5$ and a PV cylinder radius $r_0 = 1$. Inside the cylinder, $\tilde{\zeta} \simeq 0.22$. The stratification anomaly $\mathscr{D}_z$ has a distribution similar to $\tilde{\zeta}$ and is not shown. Remarkably, the vertical vorticity changes sign only in the upper region of the bisectrix, approximately, where $\tilde{\zeta} < 0$ outside the cylinder. The vertical vorticity continues positive outside the cylinder in the lower region. The nonlinear term $\tilde{\boldsymbol{\omega}} \cdot \nabla \mathscr{D}$ (figure 1b) has a radial distribution and is always positive outside the cylinder. This nonlinear term is almost everywhere smaller than the linear terms $|\tilde{\zeta}|$ and $|\mathscr{D}_z|$ (note the different contour intervals in figures 1a and 1b). The exception occurs in the region along the bisectrix, where $\tilde{\zeta} \simeq 0$, and the nonlinear term is larger than $|\tilde{\zeta}|$ and $|\mathscr{D}_z|$ (see distribution of $|\tilde{\zeta}| - |\tilde{\boldsymbol{\omega}} \cdot \nabla \mathscr{D}|$ in figure 1c). Thus, the relative importance of the nonlinear terms in the PV definition depends not only on the smallness of the Rossby number (which is here 0 since the flow is exactly geostrophic), but also on the flow location relative to the shear zone.

The margin of static instability ($\mathscr{D}_z \to 1$) occurs inside the PV cylinder when $\varpi_0 \to -1$, which coincides also with the margin of inertial instability for negative vorticity flow ($\tilde{\zeta} \to -1$). This situation is shown in figure 2 which displays the case $\varpi_0 = -0.99$. The cylinder interior is close to the inertial and static instability, with large horizontal gradients of $\tilde{\zeta}$ at the surface (figure 2a), and large vertical gradients

https://doi.org/10.1017/S0022112008003364 Published online by Cambridge University Press

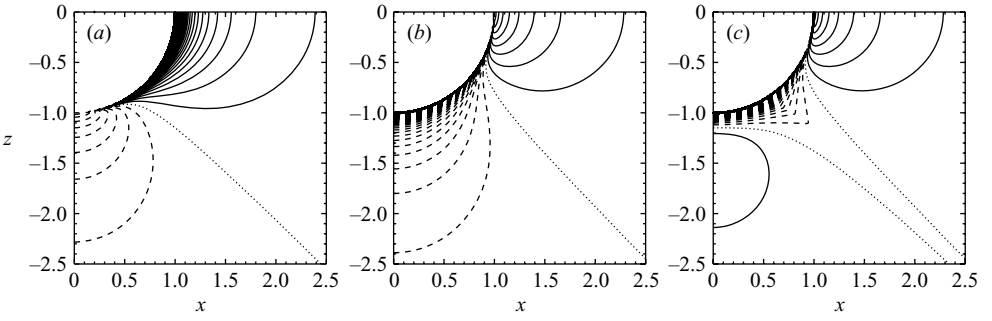


FIGURE 2. Distributions in the $(x, \hat{z})$-plane, in the case of $\varpi_0 = -0.99$, of (*a*) $\tilde{\zeta}$, (*b*) $\mathscr{D}_z$, and (*c*) the difference $|\tilde{\zeta}| - |\tilde{\boldsymbol{\omega}} \cdot \nabla \mathscr{D}|$. Contour interval $\Delta = 0.1$.

of $\mathscr{D}$ below the vortex (figure 2*b*). The nonlinear term becomes now larger than $|\tilde{\zeta}|$ and $|\mathscr{D}_z|$ over a wider area around the PV cylinder (figure 2*c*) in comparison with the case $\varpi_0 = 0.5$ (figure 1*c*). Positive ϖ_0 can increase limitlessly, though restriction to inertially stable flows ($|\tilde{\zeta}| < 1$) implies the upper limit $\varpi_0 = 3$. In this work, we consider static and inertially stable flows typical of mesoscale balanced geophysical dynamics in which $|\varpi| < 1$.

The pressure $\Phi(r)$ can be obtained from the integration of $\Psi_r(r)$, (3.12), using the integral rule

$$\int \sqrt{x^2 \pm a^2}\, \mathrm{d}x = \tfrac{1}{2} x \sqrt{x^2 \pm a^2} \pm \tfrac{1}{2} a^2 \ln\left(x + \sqrt{x^2 \pm a^2}\right), \tag{3.15}$$

which is valid for positive and negative values of ϖ_0. The integration constant is found from the continuity condition of Φ at $r = r_0$, $\Phi_i(r_0) = \Phi_e(r_0)$. Recovering the pressure Φ from (3.5), the interior (Φ_i) and exterior (Φ_e) solutions for Φ are

$$\Phi(r) = \begin{cases} \Phi_i(r) = \tfrac{1}{2}(\sqrt{\Pi_0} - 1) r^2, & r \leqslant r_0, \\ \Phi_e(r) = \tfrac{1}{2}(\sqrt{r^2 + \varpi_0 r_0^2} - r) r + \tfrac{1}{2} \varpi_0 r_0^2 \ln\left(\dfrac{r + \sqrt{r^2 + \varpi_0 r_0^2}}{r_0(1 + \sqrt{\Pi_0})}\right), & r > r_0, \end{cases} \tag{3.16}$$

where a constant pressure $\Phi(0)$ has been omitted.

We may now define the PV intensity I_0 of the PV cylinder as the amount of PV anomaly inside a section of area $A = \pi r_0^2$ of the PV cylinder with length π^{-1},

$$I_0 = \pi^{-1} \int_A \varpi \, \mathrm{d}a = 2\varpi_0 \int_0^{r_0} r \mathrm{d}r = \varpi_0 r_0^2. \tag{3.17}$$

In order to obtain the potential $\Phi_l(r)$ of a line PV vortex, we take the limit of $\Phi_e(r)$ when $r_0 \to 0$ and $\varpi \to \infty$ while the intensity I_0 remains constant. From (3.16) this limit is

$$\Phi_l(r) = \tfrac{1}{2}(\sqrt{r^2 + I_0} - r) r + \tfrac{1}{2} I_0 \ln\left(\frac{r + \sqrt{r^2 + I_0}}{\sqrt{I_0}}\right) = \Phi_{l1} + \Phi_{l2}. \tag{3.18}$$

At short distances, for $r/\sqrt{I_0} \ll 1$, both terms in (3.18) contribute equally to $\Phi_l(r)$ in a linear way,

$$\Phi_l(r) \simeq \tfrac{1}{2}\sqrt{I_0} r + \tfrac{1}{2}\sqrt{I_0} r = \sqrt{I_0} r, \quad r \ll \sqrt{I_0}, \tag{3.19}$$

https://doi.org/10.1017/S0022112008003364 Published online by Cambridge University Press

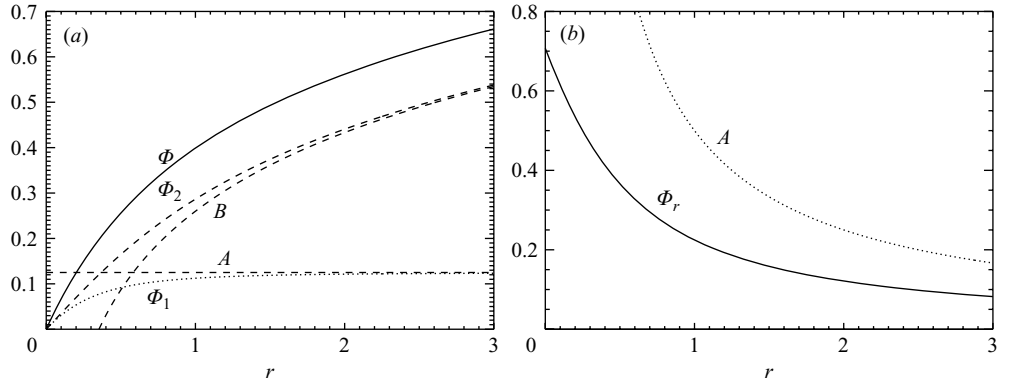


FIGURE 3. (*a*) The pressure potential $\Phi_l(r)$ (symbol Φ) of the line PV vortex with $I_0 = 0.5$, and the contributions Φ_{l1} (Φ_1) and Φ_{l2} (Φ_2) defined in (3.18). The asymptotes $I_0/4$ (A) and $\frac{1}{2} I_0 \ln(2r/\sqrt{I_0})$ (B) are included. (*b*) The corresponding pressure gradient $\Phi_{lr}(r)$ given by (3.20), and the asymptote I_0/r (A).

whereas at long distances, for $r/\sqrt{I_0} \gg 1$, the first term Φ converges asymptotically to $I_0/4$ and the second term tends to infinity as $\frac{1}{2} I_0 \ln(2r/\sqrt{I_0})$ (figure 3*a*).

The dynamically relevant quantity, however, is the pressure gradient of the line PV vortex Φ_{lr}, which is obtained from (3.12),

$$\Phi_{lr}(r) = \sqrt{r^2 + I_0} - r. \tag{3.20}$$

In the limit $r \to \infty$, the pressure gradient $\Phi_{lr}(r)$ tends to 0 as I_0/r (figure 3*b*). The important point is that, for (3.20) to be valid everywhere, I_0 must be positive. This severe restriction in the line PV vortex when $I_0 < 0$ is related to the fact that as $\varpi_0 = I_0/r_0^2 \to -\infty$ and $r_0 \to 0$ the total PV Π_0 becomes negative, which is not allowed by solution (3.10). At distances shorter than a critical $r_c = \sqrt{-\varpi_0 r_0^2}$, the flow becomes statically unstable and leaves the regime of balance flow. Thus, if the concept of line PV vortex is to be useful to the balance dynamics, it seems that an alternative approach is to impose a small but finite limit to the radius of the PV cylinders. This approach may be particularly useful in computational fluid dynamics where the finite amount of computational memory always imposes a finite numerical grid-size, and therefore there is always a limited spatial resolution. PV cylinders with a finite radius r_0 smaller than the grid-size may be considered, for computation, as one-dimensional lines. In the following sections similar ideas are developed in the most practical case of PV spheres in three-dimensional space, which lead to the concept of small PV balls.

4. The piecewise constant symmetric PV vortex

In this section, we consider the steady and horizontal motion of a three-dimensional vortex in which the centripetal acceleration plus the Coriolis acceleration is equal to the pressure gradient term (cyclostrophic balance). We use cylindrical coordinates (r, ϕ, z), where now $r^2(x, y) \equiv x^2 + y^2$ must be distinguished from the polar coordinates $(r^2(x, \hat{z}) \equiv x^2 + \hat{z}^2)$ used in the previous section. The dependent variables are the transverse (azimuthal) velocity v, $\mathscr{D}$ and Φ, since the radial and vertical velocities $u = w = 0$. The flow satisfies (2.4) which in this case is reduced to the balance of

https://doi.org/10.1017/S0022112008003364 Published online by Cambridge University Press

momentum along r, and the hydrostatic condition,

$$\frac{\tilde{v}^2}{r} + \tilde{v} = \Phi_r, \tag{4.1a}$$

$$0 = \Phi_z + c^2 \mathscr{D}, \tag{4.1b}$$

where, similarly to (3.2), we have defined the scaled pressure anomaly

$$\Phi(r, z) \equiv \frac{\alpha_0}{f^2} \mathscr{P}(r, z), \tag{4.2}$$

which includes the planetary centripetal potential term $-r^2/8$.

The solutions of $\tilde{v}$ and $\mathscr{D}$ in terms of $\Phi(r, z)$ are

$$\tilde{v} = \frac{r}{2}\left(\sqrt{1 + 4\frac{\Phi_r}{r}} - 1\right), \quad \mathscr{D} = -\epsilon^2 \Phi_z, \tag{4.3}$$

where the positive root in the expression for $\tilde{v}$ has been taken to ensure that $\tilde{v} = 0$ when $\Phi_r = 0$. It is assumed therefore, for (4.1) to have real solutions, that $1 + 4\Phi_r/r > 0$.

In this three-dimensional case, the PV anomaly definition (2.13) of the $\hat{\boldsymbol{k}}$-axis symmetrical vortex can be written in cylindrical coordinates (r, z) as

$$\Pi - 1 = \varpi = \tilde{\zeta} - \mathscr{D}_z - \tilde{\xi}\mathscr{D}_r - \tilde{\zeta}\mathscr{D}_z, \tag{4.4}$$

where $\tilde{\xi} = -\tilde{v}_z$ is the radial component of vorticity. In terms of the pressure anomaly Φ, the contributions to ϖ are

$$\tilde{\zeta} = \frac{1 + 3\Phi_r/r + \Phi_{rr}}{\sqrt{1 + 4\Phi_r/r}} - 1, \tag{4.5a}$$

$$\mathscr{D}_z = -\Phi_{\hat{z}\hat{z}}, \tag{4.5b}$$

$$\tilde{\xi}\mathscr{D}_r = \frac{\Phi_{r\hat{z}}^2}{\sqrt{1 + 4\Phi_r/r}}, \tag{4.5c}$$

$$\tilde{\zeta}\mathscr{D}_z = \left(1 - \frac{1 + 3\Phi_r/r + \Phi_{rr}}{\sqrt{1 + 4\Phi_r/r}}\right) \Phi_{\hat{z}\hat{z}}. \tag{4.5d}$$

Above we assume also that $1 + 4\Phi_r/r \neq 0$. In the particular case $\Phi_r = -r/4$, the flow $\tilde{v} = -r/2$ is barotropic (independent of z) and the relative vorticity $\tilde{\zeta} = -1$, so that $\zeta = -f$, meaning that the fluid is motionless relative to the inertial reference frame. Note that in this case $\Phi_r = -r/4 = -\partial(r^2/8)/\partial r$ is due to the planetary centripetal acceleration. The horizontal pressure gradient p_r is zero.

The sum of the terms above leads to the relation between PV and pressure gradient,

$$\Pi\sqrt{1 + 4\frac{\Phi_r}{r}} = 1 + \Phi_{rr} + \Phi_{\hat{z}\hat{z}} + \Phi_{rr}\Phi_{\hat{z}\hat{z}} - \Phi_{r\hat{z}}^2 + 3\frac{\Phi_r}{r}(1 + \Phi_{\hat{z}\hat{z}}). \tag{4.6}$$

Solution of this PV inversion equation is at the core of the piecewise constant symmetric PV vortex problem. This equation can be written more compactly in terms of the potential

$$\Psi \equiv \Phi + \tfrac{1}{2}R^2, \tag{4.7}$$

https://doi.org/10.1017/S0022112008003364 Published online by Cambridge University Press

where $R(r,\hat{z})\equiv\sqrt{r^2+\hat{z}^2}$ is the radius of the position vector in the $(r,\hat{z})$-space. The new potential $\Psi(r,\hat{z})$ satisfies the equation

$$\Pi\sqrt{4\frac{\Psi_r}{r}-3}=\hat{\mathrm{H}}\{\Psi\}+3\Psi_{\hat{z}\hat{z}}\left(\frac{\Psi_r}{r}-1\right), \tag{4.8}$$

where $\hat{\mathrm{H}}\{\Psi\}\equiv\Psi_{rr}\Psi_{\hat{z}\hat{z}}-\Psi_{r\hat{z}}^2$ is the Hessian operator in the $(r,\hat{z})$-space. Another possible choice for simplifying (4.6) is introducing

$$\beta(r,\bar{z})\equiv\Phi(r,\bar{z})+\frac{r^2+2\bar{z}^2}{8},\quad \bar{z}\equiv\sqrt{2}\,\hat{z}, \tag{4.9}$$

which leads to

$$\Pi\sqrt{\frac{\beta_r}{r}}=\bar{\mathrm{H}}\{\beta\}+3\frac{\beta_r}{r}\beta_{\bar{z}\bar{z}}, \tag{4.10}$$

where $\bar{\mathrm{H}}$ is the Hessian operator in the $(r,\bar{z})$-space.

We now specify, in a way similar to what we did with the PV cylinder in the previous section (see (3.9)), that the radial PV anomaly distribution is everywhere zero except inside a sphere of radius $R=R_0$, centred at the origin of the $(r,\hat{z})$-plane, where it has a constant value ϖ_0,

$$\varpi(R)=\begin{cases}\varpi_0, & R\leqslant R_0,\\ 0, & R>R_0.\end{cases} \tag{4.11}$$

In this case, (4.6) admits radial solutions $\Phi(R(r,\hat{z}))=F(R)$ if

$$\Pi_0\sqrt{1+4\frac{F'}{R}}=\left(1+2\frac{F'}{R}\right)^2+F''+\frac{F'}{R}\left(F''-\frac{F'}{R}\right)\left(1+\frac{3\hat{z}^2}{R^2}\right). \tag{4.12}$$

Therefore the condition $F''=F'/R$ is related to a possible radial solution. This solution corresponds to the interior solution Φ_i, that is with $\varpi=\varpi_0$,

$$\Phi_i(r,\hat{z})=\tfrac{1}{2}C\,R^2(r,\hat{z}), \tag{4.13}$$

where a constant pressure has been omitted and the $\frac{1}{2}$ is introduced to simplify further mathematical expresions. The parameter C depends on ϖ_0 and can be obtained by solving the polynomial equation resulting from substituting (4.13) into (4.12). After rearrangement of terms, this substitution leads to

$$\Pi_0\sqrt{1+4C}=(1+C)(1+4C). \tag{4.14}$$

Disregarding the solution $C=-1/4$, which corresponds to $\Phi_{ir}=-r/4$, (4.14) reduces to the cubic equation

$$\Pi_0^2=(1+C)^2(1+4C), \tag{4.15}$$

which has the solution

$$C(\varpi_0)=\tfrac{1}{4}\left(\sqrt[3]{1+8\Pi_0^2+4\Pi_0\sqrt{1+4\Pi_0^2}}+\sqrt[3]{1+8\Pi_0^2-4\Pi_0\sqrt{1+4\Pi_0^2}}-3\right), \tag{4.16}$$

with $\Pi_0=\varpi_0+1$.

In the vortex interior, the velocity $\tilde{v}_i$ depends linearly on r, and the vertical displacement of isopycnals $\mathscr{D}_i$ depends linearly on z,

$$\tilde{v}_i(r,z)=\tfrac{1}{2}(\sqrt{1+4C}-1)r,\quad \mathscr{D}_i(r,z)=-Cz. \tag{4.17}$$

https://doi.org/10.1017/S0022112008003364 Published online by Cambridge University Press

Thus, the interior fluid rotates as a solid body with angular velocity $\frac{1}{2}(\sqrt{1+4C}-1)$. Consequently, the vertical vorticity and stratification anomaly are constant,

$$\tilde{\zeta}_i = \tilde{v}_{ir} + \frac{\tilde{v}_i}{r} = \sqrt{1+4C} - 1, \quad \mathscr{D}_{iz} = -C, \tag{4.18}$$

and the shear vorticity ($\tilde{v}_{ir}$) and the curvature vorticity ($\tilde{v}_i/r$) equal the angular velocity. We note that $C(\varpi_0)$, as given by (4.16), increases monotonically from $C(-1) = -1/4$, and therefore the interior flow remains always inertial and statically stable as long as $\varpi_0 > -1$. The flow in the interior and exterior PV ball may however, be, baroclinically unstable to three-dimensional wave perturbations (see Nolan & Montgomery 2002). This type of instability is not considered here.

An analytical exterior solution Φ_e of (4.6), or in the modified expressions (4.8) or (4.10), was not found. The main difficulty is that, owing to the nonlinear term $3\Phi_r\Phi_{\hat{z}\hat{z}}/r$, the exterior solution does not have, unlike the interior solution, a radial dependence.

Instead, (4.6) was numerically solved using an iterative procedure in a double periodic domain with $(n_X, n_Z) = (1024, 1024)$ grid points. The extent of the model domain was $\{L_X, L_Z\} = 2\pi\{c, 1\}$, with the Prandtl ratio $c \equiv N/f = 10$. The numerical algorithm inverts the linear part of (4.6) in the spectral space, whereas the nonlinear terms are computed in the physical space in every iteration. To avoid the abrupt discontinuity in the PV anomaly distribution, we used a short cosine transition window of 4 grid points, thus effectively using

$$\varpi(R) = \begin{cases} \varpi_0, & R \leqslant R_0, \\ \frac{1}{2}\varpi_0\left\{1 + \cos\left[(R-R_0)\pi/\delta\right]\right\}, & R_0 < R < R_0 + \delta, \\ 0, & R \geqslant R_0 + \delta, \end{cases} \tag{4.19}$$

where the window width $\delta = 4 \times 2\pi/n_X$.

The steady numerical solution $\Phi_e(r, \hat{z})$ was confirmed through comparison with the three-dimensional solution obtained using a numerical model based on the full dynamics (2.4). The inviscid, non-hydrostatic, Boussinesq, f-plane model used (Dritschel & Viúdez 2003) was initialized using the PV initialization approach (Viúdez & Dritschel 2003), now necessary to avoid the initial generation of inertia–gravity waves which are permissible in the non-hydrostatic dynamics. The non-hydrostatic numerical model does not impose either steadiness or balance. Inertia–gravity waves, however, are excluded from the numerical solution of (4.6) owing to the constraints $u = w = 0$. We note that in a viscous fluid, large PV gradients, and therefore, large vorticity gradients, would enhance momentum dissipation. In such fluids, however, PV is not materially conserved and the approach of using 'charges' of PV that are advected by the background flow is impracticable.

The four contributions to the PV anomaly (4.4) obtained from the numerical solution are shown in figure 4. As occurs in the PV cylinder, $\tilde{\zeta}$ (figure 4*a*) and $\mathscr{D}_z$ (figure 4*b*) change sign only in the upper or lower half of the vortex boundary. The nonlinear terms $\tilde{\xi}\mathscr{D}_r$ and $\tilde{\zeta}\mathscr{D}_z$ (figure 4*c*) have, over the larger part of the domain, a magnitude smaller than those of $\tilde{\zeta}$ and $\mathscr{D}_z$. However, $\tilde{\xi}\mathscr{D}_r$ has an extremum at mid-depth just where $\tilde{\zeta}$ and $\mathscr{D}_z$ are close to zero. This means that $\tilde{\xi}\mathscr{D}_r$ can be more important than the linear terms, over some region at mid-depth, even for small Rossby numbers.

The different contributions in the right-hand side of the PV inversion equation (4.6) are shown as scatterplots (versus R) in figure 5. The larger contributions are

https://doi.org/10.1017/S0022112008003364 Published online by Cambridge University Press

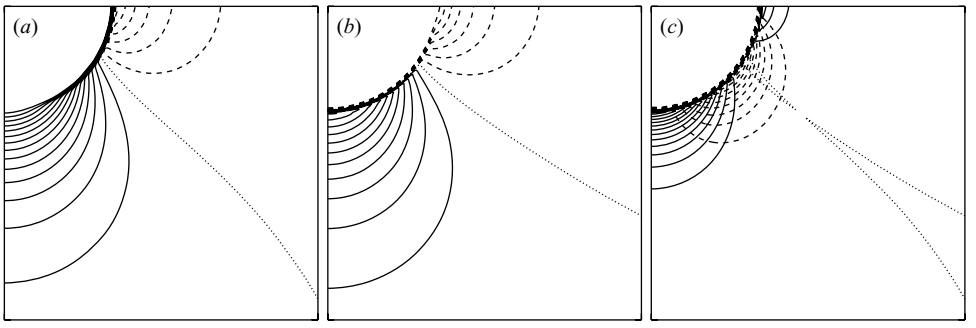


FIGURE 4. Distributions in the $(r, \hat{z})$-plane, in the case of a spherical vortex with $\varpi_0 = 0.5$ and $R_0 = 0.5$, of (*a*) $\tilde{\zeta}$ ($\Delta = 2 \times 10^{-2}$), (*b*) $\mathscr{D}_z$ ($\Delta = 2 \times 10^{-2}$), and (*c*) the nonlinear terms $-\tilde{\xi}\mathscr{D}_r$ (dashed contours, $\Delta = 5 \times 10^{-3}$) and $\tilde{\zeta}\mathscr{D}_z$ (solid contours, $\Delta = 5 \times 10^{-3}$). Domain extent is $\delta r = \delta\hat{z} = 1.5$.

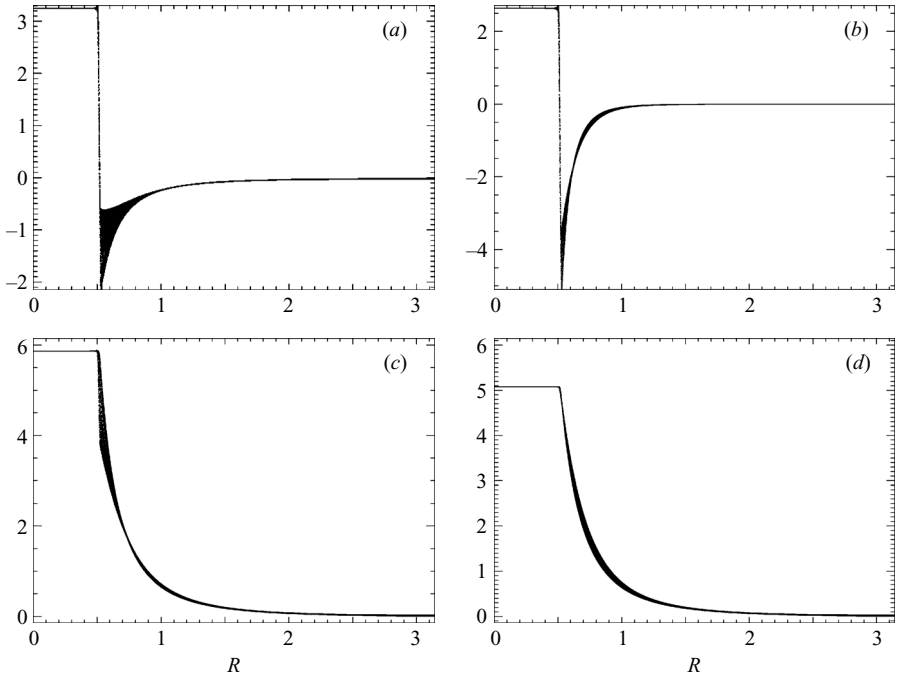


FIGURE 5. Scatterplots versus R of (*a*) $\Phi_{rr} + \Phi_{\hat{z}\hat{z}}$ ($\times 10$), (*b*) $\Phi_{rr}\Phi_{\hat{z}\hat{z}} - \Phi_{r\hat{z}}^2$ ($\times 10^2$), (*c*) $3(\Phi_r/r)(1 + \Phi_{\hat{z}\hat{z}})$ ($\times 10$), and (*d*) $3(\Phi_r/r)$ ($\times 10$).

due to the linear terms $\Phi_{rr} + \Phi_{\hat{z}\hat{z}}$ (figure 5*a*) and $3\Phi_r/r$ (figure 5*c*). The large scatter of $\Phi_{rr} + \Phi_{\hat{z}\hat{z}}$ at $R \geqslant R_0 = 0.5$ (figure 5*a*), and to a smaller degree $3\Phi_r/r$ (figure 5*c*), is a consequence of the departure of $\Phi_e(r, \hat{z})$ from radial solutions $F(R)$. This is so because if $\Phi(r, \hat{z}) = F(R(r, \hat{z}))$, the Laplacian $\Phi_{rr} + \Phi_{\hat{z}\hat{z}} = F'' + F'/R$ is a function of R alone.

Once the analytical interior solution Φ_i and the numerical exterior solution Φ_e have been found, these can be used to model dynamical systems of small PV balls. Given a PV ball defined by a parameter pair (ϖ_0, R_0), the pressure Φ, and therefore the

https://doi.org/10.1017/S0022112008003364 Published online by Cambridge University Press

induced fields of $\tilde{v}$ and $\mathscr{D}$, relevant to the velocity and vertical location of the other PV vortices, need only be computed once. The analytical external solution of (4.6) remains, however, as an important theoretical challenge. In the next two sections, we explore the PV ball vortex approach in the QG and SG approximations where analytical interior and exterior solutions are possible.

5. Quasi-geostrophic dynamics

In the QG dynamics the dependent variables (velocity $\boldsymbol{u}^q = \boldsymbol{u}_h^q + w^q\hat{\boldsymbol{k}}$, vertical displacement of isopycnals $\mathscr{D}^q$, and pressure anomaly $\mathscr{P}^q$) obey the system of equations

$$\frac{\mathrm{d}_g\boldsymbol{u}^g}{\mathrm{d}t} + f\hat{\boldsymbol{k}}\times\boldsymbol{u}_h^q = -\alpha_0\nabla_h\mathscr{P}^q, \tag{5.1a}$$

$$0 = -\alpha_0\mathscr{P}_z^q - N^2\mathscr{D}^q, \tag{5.1b}$$

$$\frac{\mathrm{d}_g\mathscr{D}^q}{\mathrm{d}t} = w^q, \tag{5.1c}$$

$$\nabla\cdot\boldsymbol{u}^q = 0, \tag{5.1d}$$

where $\boldsymbol{u}^g \equiv (\alpha/f)\hat{\boldsymbol{k}}\times\nabla_h\mathscr{P}^q$ is the geostrophic velocity, and $\mathrm{d}_g\chi/\mathrm{d}t \equiv \partial\chi/\partial t + \boldsymbol{u}^g\cdot\nabla_h\chi$ is the rate of change of χ relative to an observer moving with the geostrophic velocity. Equation (5.1*a*) is the horizontal momentum equation with the approximation that the local and advective accelerations are replaced with their respective geostrophic expressions. Equation (5.1*b*) is the hydrostatic approximation, and (5.1*c*) is the mass conservation with vertical advection neglected.

We note that, in principle, the QG variables $(\boldsymbol{u}^q, \mathscr{D}^q, \mathscr{P}^q)$ are independent of the variables $(\boldsymbol{u}, \mathscr{D}, \mathscr{P})$ of the Boussinesq flow in the previous section, and therefore all of them are labelled with a different superscript. Quantitative comparison between results from different dynamics is, however, possible only when at least two variables, one in every dynamical system, are assumed to take the same values. The choice of this common variable is often the pressure anomaly $\mathscr{P}$, though there is not any *a priori* reason that forces us to do so. A natural choice in the case of this study of PV vortices and PV inversion is the PV itself. In this respect, the geostrophic velocity $\boldsymbol{u}^g$ defined above differs also from the geostrophic velocity defined in the full or SG dynamics. We omit, however, the superscript q in the geostrophic quantities to avoid an excess of notation.

The rate of change of the dimensionless geostrophic vertical vorticity ζ^g and stratification anomaly $\mathscr{D}_z^q$ are both equal to the QG vertical velocity shear,

$$\frac{\mathrm{d}_g\tilde{\zeta}^g}{\mathrm{d}t} = \frac{\mathrm{d}_g\mathscr{D}_z^q}{\mathrm{d}t} = w_z^q, \tag{5.2}$$

and the conservation of the QG invariant anomaly ϖ_I^q follows

$$\frac{\mathrm{d}_g\varpi_I^q}{\mathrm{d}t} = 0, \quad \varpi_I^q \equiv \tilde{\zeta}^g - \mathscr{D}_z^q = \nabla_h^2\Phi^q + \frac{\partial^2\Phi^q}{\partial\hat{z}^2} = \hat{\nabla}^2\Phi^q, \quad \Phi^q \equiv \frac{\alpha_0}{f^2}\mathscr{P}^q. \tag{5.3a–c}$$

The term 'QG invariant' is used here to distinguish ϖ_I^q, as defined in (5.3*b*), from the PV anomaly of the QG flow, or QG PV, defined in the usual way from (2.13) $\varpi^q \equiv \tilde{\zeta}^q - \mathscr{D}_z^q - \tilde{\boldsymbol{\omega}}^q\cdot\nabla\mathscr{D}^q$. Sometimes ϖ_I^q is called the pseudo-PV or QG PV anomaly (Charney 1971; White 2002; Holton 2004).

https://doi.org/10.1017/S0022112008003364 Published online by Cambridge University Press

In the case of an axis-symmetric horizontal vortex the QG equations (5.1) in cylindrical coordinates reduce to

$$\frac{\tilde{v}^{g2}}{r} + \tilde{v}^q = \Phi^q_r, \tag{5.4a}$$

$$0 = \Phi^q_z + c^2 \mathscr{D}^q, \tag{5.4b}$$

$$u^q = w^q = 0. \tag{5.4c}$$

In this case the geostrophic velocity, vertical vorticity and stratification anomaly are

$$\tilde{v}^g = \Phi^q_r, \quad \tilde{\zeta}^g = \frac{(r\tilde{v}^g)_r}{r} = \tilde{v}^g_r + \frac{\tilde{v}^g}{r} = \Phi^q_{rr} + \frac{\Phi^q_r}{r}, \quad \mathscr{D}^q_z = -\Phi^q_{\hat{z}\hat{z}}. \tag{5.5}$$

For its further use we obtain from (5.4) the QG velocity, and hence the QG vertical vorticity, in terms of geostrophic quantities,

$$\tilde{v}^q = \tilde{v}^g - \frac{\tilde{v}^{g2}}{r}, \quad \tilde{\zeta}^q = \tilde{\zeta}^g - 2\tilde{v}^g_r \frac{\tilde{v}^g}{r}, \tag{5.6}$$

where the second term in every expression above can be interpreted as a small correction to the corresponding geostrophic value.

Once the basic equations have been set, we address next the flow induced by balls of constant QG invariant ϖ^q_I as well as constant QG PV ϖ^q. The first case is relevant in a QG dynamics of PV ball vortices (where ϖ^q_I is a material invariant), whereas the second case is useful as the QG approximation to the flow induced by PV ball vortices in the Boussinesq dynamics (where the material invariant $\varpi \simeq \varpi^q$).

5.1. *Flow generated by a sphere of constant QG invariant*

The expressions (5.5) imply that the QG invariant anomaly (5.3*b*) is

$$\varpi^q_I = \Phi^q_{rr} + \frac{\Phi^q_r}{r} + \Phi^q_{\hat{z}\hat{z}}. \tag{5.7}$$

For a spherical distribution of $\varpi^q_I(R)$ in the vertically stretched space $(r, \hat{z})$, the ϖ^q_I inversion equation (5.3*b*) admits radial solutions

$$\Phi^q(r, \hat{z}) = F(R), \quad R^2(r, \hat{z}) \equiv r^2 + \hat{z}^2, \quad \Rightarrow \quad \varpi^q_I = F'' + 2\frac{F'}{R}. \tag{5.8a–c}$$

In the case of a ball of radius R_0 with constant $\varpi^q_I = \varpi_0$ the interior solution Φ^q_i and its gradient $\Phi^{q\prime}_i$ are

$$\Phi^q_i(R) = \tfrac{1}{2} C^q_I R^2, \quad \Phi^{q\prime}_i(R) = C^q_I R, \quad C^q_I(\varpi_0) = \frac{1}{3}\varpi_0, \tag{5.9a–c}$$

where an irrelevant pressure constant $\Phi^q(0)$ has been omitted (5.9*a*). The exterior solution, outside the sphere where $\varpi^q_I = 0$, is obtained from (5.8*c*), defining $G \equiv F'$, leading to a separable equation which can be integrated

$$\int \frac{\mathrm{d}G}{G} = -2\int \frac{\mathrm{d}R}{R} \quad \Rightarrow \quad G(R) = \frac{G_0}{R^2} \quad \Rightarrow \quad F(R) = \frac{F_0}{R} + F_1. \tag{5.10}$$

The integration constants are obtained by imposing continuity of Φ^q and $\Phi^{q\prime}$ at $R = R_0$, yielding the exterior pressure and pressure gradient solutions

$$\Phi^q_e(R) = \Phi^q_0 + \frac{\varpi_0 R_0^2}{2} - \frac{\varpi_0 R_0^3}{3R}, \quad \Phi^{q\prime}_e(R) = \frac{\varpi_0 R_0^3}{3R^2}. \tag{5.11a, b}$$

https://doi.org/10.1017/S0022112008003364 Published online by Cambridge University Press

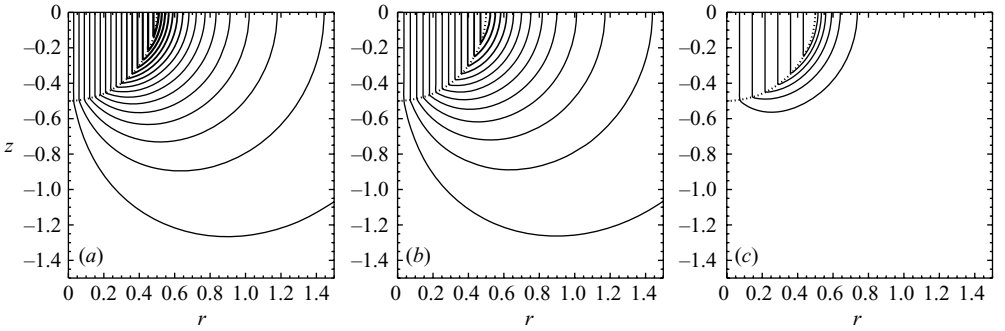


FIGURE 6. Distributions in the $(r, \hat{z})$-plane, in the case of $\varpi_I^q = 0.5$ and $R_0 = 0.5$, of (a) $\tilde{v}^g$ $(\max\{\tilde{v}^g\} = 0.083, \Delta = 5 \times 10^{-3})$, (b) $\tilde{v}^q$ $(\max\{\tilde{v}^q\} = 0.069, \Delta = 5 \times 10^{-3})$, and (c) the difference $\tilde{v}^g - \tilde{v}^q$ $(\max\{\tilde{v}^g - \tilde{v}^q\} = 0.014, \Delta = 2 \times 10^{-3})$. The dotted line indicates the location of the PV vortex. Domain extent is $\delta r = \delta\hat{z} = 1.5$.

These QG interior and exterior solutions were obtained by Thorpe & Bishop (1994) (also reproduced in Holton 2004, § 6.3.4). Using the chain rule $\chi_r = \chi' \, \partial R/\partial r = \chi' \, r/R$, we obtain the geostrophic velocity and vertical vorticity

$$\tilde{v}^g = \begin{cases} \dfrac{\varpi_0}{3} r, & \\ \dfrac{\varpi_0 R_0^3}{3} \dfrac{r}{R^3}, & \end{cases} \qquad \tilde{\zeta}^g = \begin{cases} \dfrac{2\varpi_0}{3}, & R \leqslant R_0, \\ \dfrac{\varpi_0 R_0^3}{3} \dfrac{1}{R^3} \left(2 - \dfrac{3r^2}{R^2}\right), & R > R_0. \end{cases} \tag{5.12a, b}$$

The relations between QG and geostrophic quantities (5.6) can be written, using (5.9) and (5.11), in terms of the constant QG invariant anomaly $\varpi_I^q = \varpi_0$ as

$$\tilde{v}^q = \begin{cases} \dfrac{\varpi_0}{3} \left(1 - \dfrac{\varpi_0}{3}\right) r, & R \leqslant R_0, \\ \dfrac{\varpi_0 R_0^3}{3} \dfrac{r}{R^3} \left(1 - \dfrac{\varpi_0 R_0^3}{3R^3}\right), & R > R_0, \end{cases} \tag{5.13}$$

and

$$\tilde{\zeta}^q = \begin{cases} \dfrac{2\varpi_0}{3} \left(1 - \dfrac{\varpi_0}{3}\right), & R \leqslant R_0, \\ \dfrac{\varpi_0 R_0^3}{3R^3} \left(2 - \dfrac{3r^2}{R^2}\right) - 2 \left(\dfrac{\varpi_0 R_0^3}{3R^3}\right)^2 \left(1 - \dfrac{3r^2}{R^2}\right), & R > R_0. \end{cases} \tag{5.14}$$

The interior QG vortex rotates therefore with an angular velocity equal to $\varpi_0(3 - \varpi_0)/9$. The distributions of $\tilde{v}^g$, $\tilde{v}^q$ and $\tilde{v}^g - \tilde{v}^q$ for $\varpi_I^q = 0.5$ and $R_0 = 0.5$ are shown in figure 6. As can be deduced from (5.12*a*) and (5.13), $\tilde{v}^q$ differs from $\tilde{v}^g$ in the interior and exterior of the vortex, the interior difference being $\tilde{v}^g - \tilde{v}^q$ a solid body rotation of angular velocity $(\tilde{\zeta}^g - \tilde{\zeta}^q)/2 = (\varpi_0/3)^2$. This difference is independent of the sign of ϖ, so that cyclones $(\tilde{v}^q > 0)$ are always subgeostrophic and anticyclones $(\tilde{v}^q < 0)$ are always supergeostrophic. In both cases $\tilde{v}^g > \tilde{v}^q$. The geostrophic and QG vertical vorticity (figure 7*a*, *b*) are qualitatively similar to the vertical vorticity found in the Boussinesq dynamics (figure 4*a*), with the change of sign happening only in the upper half of the vortex. The $\tilde{\zeta}^q$ (figure 7*b*) has, however, a small relative extreme at the surface close to the PV boundary that is not found either in the total $\tilde{\zeta}$ or in $\tilde{\zeta}^g$.

https://doi.org/10.1017/S0022112008003364 Published online by Cambridge University Press

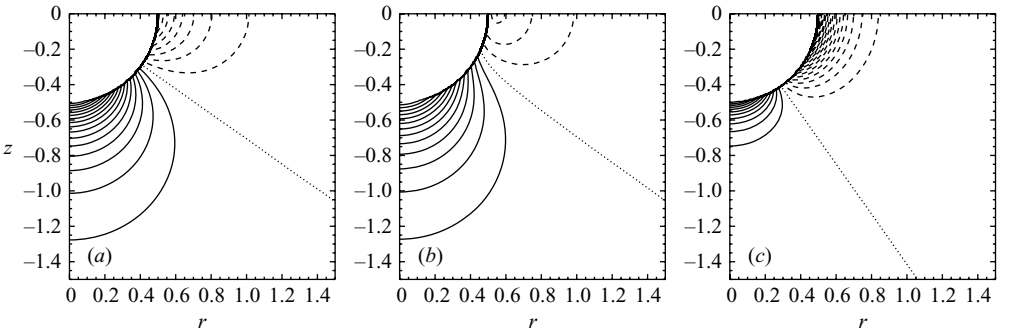


FIGURE 7. Distributions in the $(r, \hat{z})$-plane, in the case of $\varpi_0^q = 0.5$ and $R_0 = 0.5$, of (a) $\tilde{\zeta}^g$ ($\tilde{\zeta}^g \in [-0.17, 0.33]$, $\Delta = 2 \times 10^{-2}$), (b) $\tilde{\zeta}^q$ ($\tilde{\zeta}^q \in [-0.062, 0.28]$, $\Delta = 2 \times 10^{-2}$), and (c) the difference $\Delta\tilde{\zeta} \equiv \tilde{\zeta}^g - \tilde{\zeta}^q$ ($\Delta\tilde{\zeta} \in [-0.11, 0.056]$, $\Delta = 5 \times 10^{-3}$).

The external pressure gradient (5.11b) may be written as

$$\Phi_e^{q\prime}(R) = \frac{I_0}{4\pi R^2}, \quad I_0 \equiv \frac{4}{3}\pi R_0^3 \varpi_0, \tag{5.15a, b}$$

where I_0 is the amount of ϖ_I^q inside the sphere. For a given I_0, inertial and static instability occurs, as $R \to 0$ and $\varpi_0 \to \infty$. For example, the ratio between centripetal and Coriolis accelerations is

$$\frac{\tilde{v}^{g2}/r}{|\tilde{v}^q|} = \frac{|\tilde{v}^g|}{|r - \tilde{v}^g|} < 1 \quad \Leftrightarrow \quad \frac{\tilde{v}^g}{r} < \tfrac{1}{2} \quad \Leftrightarrow \quad \varpi_0 < \tfrac{3}{2}. \tag{5.16}$$

Thus, for any I_0, inertial instability occurs at distances shorter than $R < \sqrt[3]{I_0/(2\pi)}$. In terms of I_0, the vertical vorticity and stratification generated by a point QG vortex are

$$\tilde{\zeta}^g = \mathscr{D}_z^q = \frac{I_0}{4\pi R^3}\left(\frac{3\hat{z}^2}{R^2} - 1\right) = \frac{I_0}{4\pi R^3}\left(2 - \frac{3r^2}{R^2}\right), \tag{5.17}$$

which shows that static instability ($\mathscr{D}_z^q > 1$) occurs at $r = 0$ at shallow depths $|z| < \sqrt[3]{I_0/(2\pi)}$. Based on these instability arguments, the point QG vortex always generates a flow incompatible with the dynamics of typical mesoscale balanced flows. It is in this sense that the PV ball QG vortex may be more useful. In § 6, we will explore the same concept, but in the SG dynamics.

5.2. *Flow generated by a sphere of constant QG PV*

In this case the constant value ϖ_0 inside the vortex corresponds to a constant QG PV $\varpi^q = \varpi_0$ defined by (4.4) rather than to a constant value of the QG invariant ϖ_I^q defined by (5.3b). From (2.13) the PV anomaly of the QG flow is

$$\varpi^q = \tilde{\zeta}^q - \mathscr{D}_z^q - \tilde{\xi}^q \mathscr{D}_r^q - \tilde{\zeta}^q \mathscr{D}_z^q. \tag{5.18}$$

Using (5.5) and (5.6) the relation between π^q and the QG pressure Φ^q is

$$\Pi^q = \left(1 + \Phi_{rr}^q + \Phi_{\hat{z}\hat{z}}^q + \Phi_{rr}^q \Phi_{\hat{z}\hat{z}}^q - \Phi_{r\hat{z}}^{q2}\right)\left(1 - 2\frac{\Phi_r^q}{r}\right) + 3\frac{\Phi_r^q}{r}\left(1 + \Phi_{\hat{z}\hat{z}}^q\right). \tag{5.19}$$

https://doi.org/10.1017/S0022112008003364 Published online by Cambridge University Press

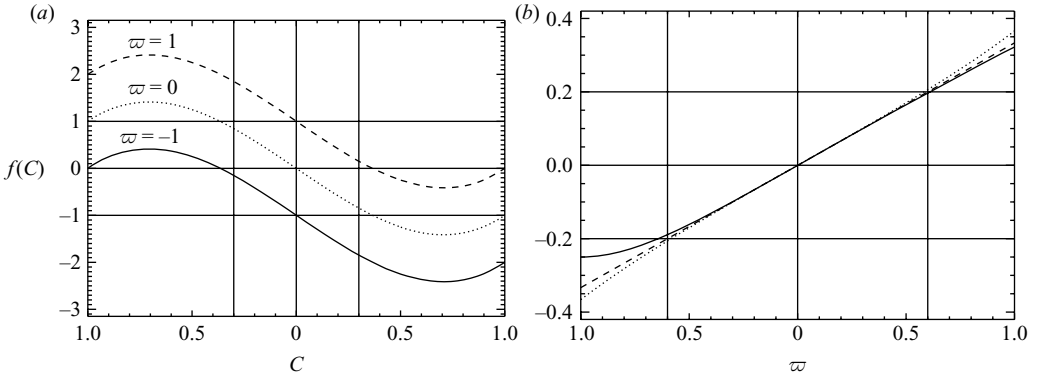


FIGURE 8. (*a*) The function $f(C) = 2C^3 - 3C + \varpi$, for $\varpi \in \{-1, 0, 1\}$. (*b*) The coefficients $C(\varpi)$ (dashed line), $C_I^q(\varpi)$ (continuous line), and $C^q(\varpi)$ (dotted line).

Radial solutions $\Phi^q(r, \hat{z}) = F(R(r, \hat{z}))$ must satisfy

$$\Pi^q = [1 + F'' + G + G(F'' - G) + G^2](1 - 2G) + 3G\left(G + \frac{\hat{z}^2}{R^2}(F'' - G) + 1\right), \quad (5.20)$$

where $G \equiv F'/R$. Radial solutions are therefore possible as long as $F'' = F'/R$, which correspond to interior solutions

$$\Phi_i^q(R) = \tfrac{1}{2}C^q R^2. \quad (5.21)$$

Substituting (5.21) into (5.20) we obtain the equation for C^q,

$$2C^{q3} - 3C^q + \varpi_0 = 0. \quad (5.22)$$

This depressed cubic equation has three different roots, corresponding to the three solutions of the cubic root of a complex number. However, the only root related to stable flow is the one closer to $C^q = 0$, which is the solution for $\varpi_0 = 0$ (see figure 8*a*). This solution is

$$C^q(\varpi_0) = \sqrt{2}\cos\frac{\theta(\varpi_0) + i2\pi}{3}, \quad \theta(\varpi_0) = \arctan\frac{\sqrt{2 - \varpi_0^2}}{-\varpi_0}, \quad -\pi \leqslant \theta < \pi, \quad (5.23)$$

where $i = 1$ ($\varpi_0 > 0$) and $i = 2$ ($\varpi_0 < 0$). For small ϖ_0, the following approximation and series expansions can be taken

$$\frac{\sqrt{2 - \varpi_0^2}}{\varpi_0} \cong \frac{\sqrt{2}}{\varpi_0}, \quad \arctan x \cong \pm\frac{\pi}{2} - \frac{1}{x}, (\pm x > 1), \quad \sin x \cong x, \quad (5.24)$$

leading to

$$C^q(\varpi_0) \cong \sqrt{2}\cos\left(\frac{3\pi}{2} + \frac{\varpi_0}{3\sqrt{2}}\right) = \sqrt{2}\sin\left(\frac{\varpi_0}{3\sqrt{2}}\right) \cong \frac{\varpi_0}{3}, \quad (5.25)$$

which is equal to the interior pressure generated by a ball of QG invariant $\varpi_I^q = \varpi_0$ (5.9*c*). The three coefficients of the interior solution seen so far, the exact C, and the QG coefficients C_I^q and C^q are plotted in figure 8(*b*) as functions of ϖ. For $|\varpi| < 1$ they are close to the QG slope equal to 1/3.

https://doi.org/10.1017/S0022112008003364 Published online by Cambridge University Press

6. Semi-geostrophic dynamics

In the SG dynamics (Eliassen 1949; Fjortoft 1962; Hoskins 1975; Hoskins & Draghici 1977) the SG dependent variables $(\boldsymbol{u}^s, \mathscr{D}^s, \mathscr{P}^s)$ satisfy

$$\frac{\mathrm{d}_s \boldsymbol{u}^g}{\mathrm{d}t} + f\hat{\boldsymbol{k}} \times \boldsymbol{u}^s = -\alpha_0 \nabla_h \mathscr{P}^s, \tag{6.1a}$$

$$0 = -\alpha_0 \mathscr{P}^s_z - N^2 \mathscr{D}^s, \tag{6.1b}$$

$$\frac{\mathrm{d}_s \mathscr{D}^s}{\mathrm{d}t} = w^s, \tag{6.1c}$$

$$\nabla \cdot \boldsymbol{u}^s = 0, \tag{6.1d}$$

where the geostrophic velocity $\boldsymbol{u}^g \equiv (\alpha_0/f)\hat{\boldsymbol{k}} \times \nabla_h \mathscr{P}^s$, and $\mathrm{d}_s\chi/\mathrm{d}t \equiv \partial\chi/\partial t + \boldsymbol{u}^s \cdot \nabla\chi$ is the rate of change of χ experienced by an observed flow moving with the SG velocity $\boldsymbol{u}^s$. In the steady horizontal flow of a spherical vortex, and in cylindrical coordinates, (6.1) reduce to

$$\frac{\tilde{v}^s \tilde{v}^g}{r} + \tilde{v}^s = \Phi^s_r, \tag{6.2a}$$

$$\mathscr{D}^s = -\epsilon^2 \Phi^s_z, \tag{6.2b}$$

$$u^s = w^s = 0, \tag{6.2c}$$

where the geostrophic velocity $\tilde{v}^g = \Phi^s_r$. The relation between $\tilde{v}^s$ and $\tilde{v}^g$ in the SG dynamics is therefore

$$\tilde{v}^s = \tilde{v}^g \left(1 + \frac{\tilde{v}^g}{r}\right)^{-1}, \tag{6.3}$$

where we assume $\tilde{v}^g \neq -r$, that is, $\Phi^s_r \neq 0$ except at $r = 0$.

The relations between the SG vertical vorticity and stratification anomaly as a function of the SG pressure are

$$\tilde{\zeta}^s = \tilde{v}^s_r + \frac{\tilde{v}^s}{r} = \left(1 + \frac{\Phi^s_r}{r}\right)^{-2} \left[\Phi^s_{rr} + \frac{\Phi^s_r}{r}\left(1 + 2\frac{\Phi^s_r}{r}\right)\right], \tag{6.4a}$$

$$\mathscr{D}^s_z = -\Phi^s_{\tilde{z}\tilde{z}}. \tag{6.4b}$$

These expressions are used next to express the SG invariant and SG PV as a function of Φ^s.

6.1. *Flow generated by a sphere of constant SG invariant*

The material invariant of the SG flow (Hoskins 1975) can be interpreted in terms of the vorticity–velocity gradient cofactor tensor (Viúdez 2005) and expressed in tensor notation as

$$\Pi^s_I \equiv \nabla d^s \cdot \boldsymbol{\Xi}^s \cdot \hat{\boldsymbol{k}}, \tag{6.5}$$

where $\boldsymbol{\Xi}^s$ is the SG approximation to the vorticity–velocity gradient cofactor tensor. This SG tensor is defined as

$$\boldsymbol{\Xi}^s \equiv (\tilde{\boldsymbol{\omega}}^g + \hat{\boldsymbol{k}})\hat{\boldsymbol{k}} + \tfrac{1}{2}\nabla\tilde{\boldsymbol{u}}^g \times\!\!\times \nabla\tilde{\boldsymbol{u}}^g. \tag{6.6}$$

The second term on the right-hand side in (6.6) is the cofactor tensor of $\tilde{\boldsymbol{u}}^g$, sometimes also denoted as $\overline{\nabla\tilde{\boldsymbol{u}}^g}$. For two vectors $\boldsymbol{a}$ and $\boldsymbol{b}$ whose Cartesian components are (a_1, a_2, a_3) and (b_1, b_2, b_3), respectively, we define the double-cross-product of tensors $\nabla\boldsymbol{a} = \nabla a_i\, \hat{\boldsymbol{e}}_i = \hat{\boldsymbol{e}}_i\, \boldsymbol{a}_{,i}$ and $\nabla\boldsymbol{b} = \nabla b_j\, \hat{\boldsymbol{e}}_j = \hat{\boldsymbol{e}}_j\, \boldsymbol{b}_{,j}$ (summation convention assumed) as

$$\nabla\boldsymbol{a} \times\!\!\times \nabla\boldsymbol{b} = \nabla a_i \times \nabla b_j\ \hat{\boldsymbol{e}}_i \times \hat{\boldsymbol{e}}_j = \hat{\boldsymbol{e}}_i \times \hat{\boldsymbol{e}}_j\ \ \boldsymbol{a}_{,i} \times \boldsymbol{b}_{,j}, \tag{6.7}$$

https://doi.org/10.1017/S0022112008003364 Published online by Cambridge University Press

where the comma-subindex notation indicates the partial derivative $(\chi_{,1},\ \chi_{,2},\ \chi_{,3}) = (\chi_{,x},\ \chi_{,y},\ \chi_{,z}) = (\partial\chi/\partial x, \partial\chi/\partial y, \partial\chi/\partial z)$. This term involves the cross-products of the gradients of the components of $\boldsymbol{a}$ and $\boldsymbol{b}$ along different directions.

In the case of the spherical vortex, the cofactor of $\nabla\tilde{\boldsymbol{u}}^g$ may be obtained directly from $\nabla\tilde{\boldsymbol{u}}^g$ in cylindrical coordinates,

$$\tfrac{1}{2}\nabla\tilde{\boldsymbol{u}}^g \overset{\times}{\times} \nabla\tilde{\boldsymbol{u}}^g = \tilde{v}_r^g \frac{\tilde{v}^g}{r}\hat{\boldsymbol{k}}\hat{\boldsymbol{k}} - \tilde{v}_z^g \frac{\tilde{v}^g}{r}\hat{\boldsymbol{r}}\hat{\boldsymbol{k}}. \tag{6.8}$$

The above result can also be obtained in Cartesian coordinates using $\tilde{\boldsymbol{u}}^g = \tilde{u}_1^g\hat{\boldsymbol{\imath}} + \tilde{u}_2^g\hat{\boldsymbol{\jmath}} = \tilde{v}^g\hat{\boldsymbol{k}} \times \hat{\boldsymbol{r}} = (-y, x)\tilde{v}^g(r(x, y), z)/r(x, y)$, and the chain rule to obtain the cofactor tensor in Cartesian coordinates from $\frac{1}{2}\nabla\tilde{\boldsymbol{u}}^g \overset{\times}{\times} \nabla\tilde{\boldsymbol{u}}^g = (\nabla\tilde{u}_1^g \times \nabla\tilde{u}_2^g)\hat{\boldsymbol{k}}$. Thus, for an axis-symmetrical vortex, the SG invariant in cylindrical coordinates is

$$\begin{aligned}\Pi_I^s = 1 + \tilde{\zeta}^g - \mathscr{D}_z - \tilde{\xi}^g\mathscr{D}_r - \mathscr{D}_z\tilde{\zeta}^g \\ + \tilde{v}_r^g\frac{\tilde{v}^g}{r}(1 - \mathscr{D}_z) + \tilde{v}_z^g\frac{\tilde{v}^g}{r}\mathscr{D}_r.\end{aligned} \tag{6.9}$$

Using (6.3) and (6.4), we replace the terms above by their expressions as functions of the SG pressure Φ^s which yields

$$\Pi_I^s = \left(1 + \Phi_{rr}^s + \Phi_{\hat{z}\hat{z}}^s + \Phi_{rr}^s\Phi_{\hat{z}\hat{z}}^s - \Phi_{r\hat{z}}^{s2}\right)\left(1 + \frac{\Phi_r^s}{r}\right). \tag{6.10}$$

As usual, we look for radial solutions $\Phi^s(r, \hat{z}) = F(R(r, \hat{z}))$ which must now satisfy

$$\begin{aligned}\Pi_I^s &= \left[1 + F'' + \frac{F'}{R}\left(1 + F'' - \frac{F'}{R}\right) + \left(\frac{F'}{R}\right)^2\right]\left(1 + \frac{F'}{R}\right) \\ &= (1 + F'')\left(1 + \frac{F'}{R}\right)^2.\end{aligned} \tag{6.11}$$

The above equation admits therefore radial solutions for both the interior and exterior vortex. The interior solutions $F_i(R) \equiv C_I^s R^2/2$ imply $F_i'' = F_i'/R = C_I^s$ and therefore

$$\Phi_i^s(R) = \tfrac{1}{2}C_I^s R^2, \quad C_I^s(\varpi_I^s) = \sqrt[3]{1 + \varpi_I^s} - 1. \tag{6.12a, b}$$

where $\varpi_I^s \equiv \Pi_I^s - 1$ is the SG invariant anomaly.

To find the exterior solution ($\Pi_I^s = 1$), we define the auxiliary function $h(R) \equiv 1 + F'(R)/R$, in terms of which (6.11) is rewritten as

$$1 = h^3 + h^2h'R. \tag{6.13}$$

This equation is separable and can be integrated,

$$\int \frac{\mathrm{d}R}{R} = \int \frac{h^2}{1 - h^3}\,\mathrm{d}h, \tag{6.14}$$

yielding

$$h(R) = \sqrt[3]{1 + \varpi_I^s\left(R_0^3/R^3\right)}. \tag{6.15}$$

The integration constant has been used to impose continuity of the internal F_i' and external F_e' solutions at $R = R_0$. Finally, the solution for the SG pressure gradient

https://doi.org/10.1017/S0022112008003364 Published online by Cambridge University Press

$\Phi^{s\prime}(R) = F'(R)$ is

$$\Phi^{s\prime}(R) = \begin{cases} \Phi_i^{s\prime}(R) = \left(\sqrt[3]{1+\varpi_I^s} - 1\right) R, & R \leqslant R_0, \\ \Phi_e^{s\prime}(R) = \left(\sqrt[3]{1+\varpi_I^s \left(R_0^3/R^3\right)} - 1\right) R, & R > R_0, \end{cases} \tag{6.16}$$

which is the solution found by Thorpe & Bishop (1995) and related to that given by Shutts (1991). The SG velocity associated to a Π_I^s sphere of radius R_0 is obtained from (6.3),

$$\tilde{v}^s(r,\hat{z}) = \begin{cases} \tilde{v}_i^s(r,\hat{z}) = \left(1 - \dfrac{1}{\sqrt[3]{1+\varpi_I^s}}\right) r, & R \leqslant R_0, \\ \tilde{v}_e^s(r,\hat{z}) = \left(1 - \dfrac{1}{\sqrt[3]{1+\varpi_I^s \left(R_0^3/R^3\right)}}\right) r, & R > R_0, \end{cases} \tag{6.17}$$

The geostrophic velocity is easily obtained from the fact that $\tilde{v}^g/r = \Phi_r^s/r = \Phi^{s\prime}/R$, and hence the SG vorticity from (6.4*a*),

$$\tilde{\zeta}^s(r,\hat{z}) = \begin{cases} \tilde{\zeta}_i^s(r,\hat{z}) = 2\left(1 - \dfrac{1}{\sqrt[3]{1+\varpi_I^s}}\right), & R \leqslant R_0, \\ \tilde{\zeta}_e^s(r,\hat{z}) = 2\left(1 - \dfrac{1}{\sqrt[3]{1+\varpi_I^s \dfrac{R_0^3}{R^3}}}\right) - \dfrac{\varpi_I^s R_0^3 r^2}{R^5 \left(1+\varpi_I^2\left(R_0^3/R^3\right)\right)^{4/3}}, & R > R_0. \end{cases} \tag{6.18}$$

The relation between the geostrophic vorticity of the SG dynamics and the pressure gradient anomaly is

$$\tilde{\zeta}^g = \Phi_{rr}^s + \frac{\Phi_r^s}{r} = 2\frac{F'}{R} + \frac{r^2}{R^2}\left(F'' - \frac{F'}{R}\right), \tag{6.19}$$

which, from (6.16), leads to the solution

$$\tilde{\zeta}^g(r,\hat{z}) = \begin{cases} \tilde{\zeta}_i^g = 2\left(\sqrt[3]{1+\varpi_I^s} - 1\right), & R \leqslant R_0, \\ \tilde{\zeta}_e^g = 2\left(\sqrt[3]{1+\varpi_I^s (R_0/R)} - 1\right) - \dfrac{\varpi_I^s}{3} \dfrac{R_0 r^2}{R^3 \left(1+\varpi_I^s (R_0/R)\right)^{2/3}}, & R > R_0. \end{cases} \tag{6.20}$$

The SG vertical vorticities $\tilde{\zeta}^s$ and $\tilde{\zeta}^g$, and the difference $\tilde{\zeta}^s - \tilde{\zeta}^g$ are plotted in figure 9. These are qualitatively similar to the corresponding QG quantities (figure 7). In the SG case, $\tilde{\zeta}^s$ has also a relative extremum at the surface (figure 9*b*).

In a similar way, we obtain the stratification anomaly of the SG dynamics,

$$\mathscr{D}_z^s = -\Phi_{\hat{z}\hat{z}}^s = -\frac{F'}{R} - \frac{\hat{z}^2}{R^2}\left(F'' - \frac{F'}{R}\right), \tag{6.21}$$

https://doi.org/10.1017/S0022112008003364 Published online by Cambridge University Press

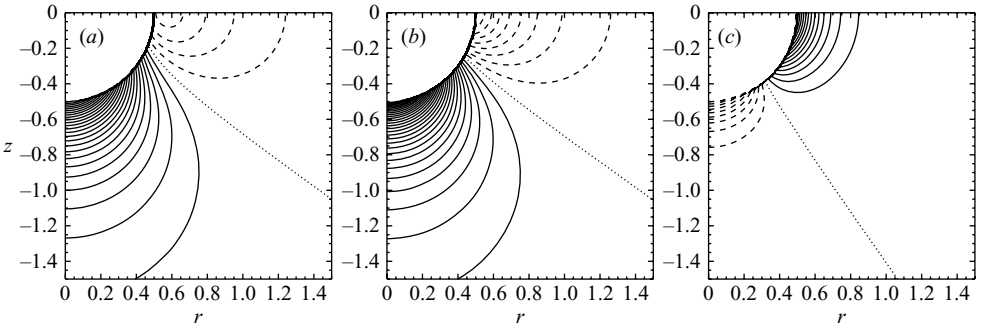


FIGURE 9. Distributions in the $(r, \hat{z})$-plane, in the case of $\varpi_I^s = 0.5$, of (*a*) $\tilde{\zeta}^s$ ($\Delta = 10^{-2}$), (*b*) $\tilde{\zeta}^g$ ($\Delta = 10^{-2}$), and (*c*) the difference $\tilde{\zeta}^s - \tilde{\zeta}^g$ ($\Delta = 4 \times 10^{-3}$).

and finally, from (6.16), the stratification anomaly in terms of the SG invariant anomaly,

$$\mathscr{D}_z^s(r, \hat{z}) = \begin{cases} \mathscr{D}_{zi}^s = 1 - \sqrt[3]{1 + \varpi_I^s}, & R \leqslant R_0, \\ \mathscr{D}_{ze}^s = 1 - \sqrt[3]{1 + \varpi_I^s \left(R_0^3/R^3\right)} + \dfrac{\varpi_I^s R_0^3 \hat{z}^2}{R^5 \left(1 + \varpi_I^s \left(R_0^3/R^3\right)\right)^{2/3}}, & R > R_0, \end{cases} \tag{6.22}$$

where $\mathscr{D}_{ze}^s$ above has been expressed so as to easily check its continuity with $\mathscr{D}_{zi}^s$ at $(r, \hat{z}) = (R_0, 0)$. Clearly, static instability ($\mathscr{D}_z^s > 1$) occurs in the vortex interior when $\varpi_I^s < -1$.

6.2. *Flow generated by a sphere of constant SG PV*

From (2.13), the PV anomaly of the SG flow is

$$\varpi^s = \tilde{\zeta}^s - \mathscr{D}_z^s - \tilde{\xi}^s \mathscr{D}_r^s - \tilde{\zeta}^s \mathscr{D}_z^s. \tag{6.23}$$

Using (6.4) and the fact that

$$\tilde{\xi}^s \mathscr{D}_r^s = \left(1 + \frac{\Phi_r^s}{r}\right)^{-2} \Phi_{r\hat{z}}^{s2}, \tag{6.24}$$

the SG PV equation (6.23) can be written in terms of Φ^s as

$$\varpi^s \left(1 + \frac{\Phi_r^s}{r}\right)^2 = \Phi_{rr}^s + \Phi_{\hat{z}\hat{z}}^s + \Phi_{rr}^s \Phi_{\hat{z}\hat{z}}^s - \Phi_{r\hat{z}}^{s2} + \frac{\Phi_r^s}{r}\left[1 + 2\frac{\Phi_r^s}{r} + 3\Phi_{\hat{z}\hat{z}}^s \left(1 + \frac{\Phi_r^s}{r}\right)\right]. \tag{6.25}$$

Looking for radial solutions $\Phi^s(r, \hat{z}) = F(R(r, \hat{z}))$, $\varpi^s(R) = \varpi_0$ for $R < R_0$, and defining $G(R) \equiv F'(R)/R$ to simplify the notation, we obtain

$$(1 + G)^2 \varpi_0 = F'' + 2G + 6G^2 + 3G^3 + G\left(F'' - G\right)\left[1 + \frac{3\hat{z}^2}{R^2}(1 + G)\right]. \tag{6.26}$$

This equation admits radial solutions when $F'' = G$, which correspond to the interior solution

$$\Phi_i^s(R) = \tfrac{1}{2} C^s R^2, \tag{6.27}$$

for which

$$\Phi_{rr}^s = \Phi_{\hat{z}\hat{z}}^s = \frac{\Phi_r^s}{r} = F'' = \frac{F'}{R} = G = C^s, \quad \Phi_{r\hat{z}}^s = 0. \tag{6.28}$$

https://doi.org/10.1017/S0022112008003364 Published online by Cambridge University Press

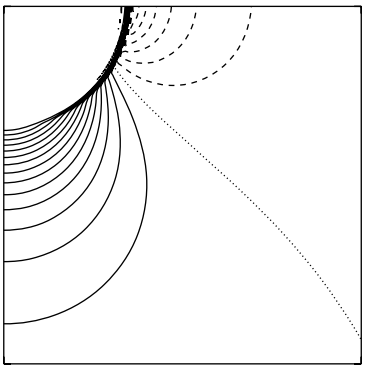


FIGURE 10. Distribution in the $(r, \hat{z})$-plane of $\tilde{\zeta}^s$ ($\Delta = 2 \times 10^{-2}$) in the case of $\varpi^s = 0.5$.

Replacing (6.27) into (6.26) and grouping terms in powers of C^s we obtain the cubic equation for the coefficient C^s

$$3C^{s3} + (6 - \varpi_0)C^{s2} + (3 - 2\varpi_0)C^s - \varpi_0 = 0. \tag{6.29}$$

Surprisingly, this equation can easily be rewritten in terms of its roots and directly solved,

$$\left(C^s - \frac{\varpi_0}{3}\right)(C^s + 1)^2 = 0, \quad \Rightarrow \quad C^s(\varpi_0) = \frac{\varpi_0}{3}. \tag{6.30}$$

The unique solution above follows since $\Phi^s_{ir} \neq -r \Rightarrow C^s \neq -1$. Thus, the SG pressure anomaly in the vortex interior has the same relation with the SG PV as the QG pressure anomaly with the QG invariant (5.9*c*).

As happens with the PV inversion equation for the total (4.6) and QG (5.19) dynamics, the exterior solution of the SG PV inversion equation (6.25) does not admit a radial dependence, which makes it difficult to find an analytical solution. Instead, (6.25) can be solved numerically using an iterative procedure similar to the one used to solved the total PV inversion (4.6). Figure 10 shows the distribution of $\tilde{\zeta}^s$ obtained from the numerical solution $\Phi^s(x, \hat{z})$ with $\varpi^s(R > 0.5) = 0.5$ which, though qualitatively similar to the $\tilde{\zeta}^s$ generated by $\varpi^s_I(R > 0.5) = 0.5$ (figure 9*a*), does not have a surface relative extremum.

7. Approximated PV equations

In the two previous sections we have considered PV and material invariant equations consistent with the QG and SG approximations to the full dynamics. Here we explore a different approach and, instead of assuming first the approximations at the level of the dynamical equations, and obtaining therefrom the approximated PV equation, the approximations are taken directly from the full PV equation (4.6) without concern for their corresponding dynamical equations.

7.1. *Quasi-linear approximation*

This approximation is based on the order of magnitude of the different terms in (4.6), for moderate PV anomalies $\varpi \cong 0.5$, which suggest that the linear terms are, by one order of magnitude, larger than the nonlinear ones (figure 5). Neglecting the nonlinear terms on the right-hand side of (4.6) yields the approximated PV equation

$$\Pi_0 \sqrt{1 + 4\frac{\Phi^a_r}{r}} = 1 + \Phi^a_{rr} + \Phi^a_{\hat{z}\hat{z}} + 3\frac{\Phi^a_r}{r}. \tag{7.1}$$

https://doi.org/10.1017/S0022112008003364 Published online by Cambridge University Press

This simplified PV equation admits radial solutions $\Phi^a(r,\hat{z}) = F(R(r,\hat{z}))$ that must satisfy

$$\Pi_0\sqrt{1+4\frac{F'}{R}} = F'' + 1 + 4\frac{F'}{R}. \tag{7.2}$$

As usual, the interior solution F_i is

$$F_i(R) = \tfrac{1}{2}C^a R^2, \tag{7.3}$$

where C^a, found by solving a quadratic equation, is

$$C^a(\varpi_0) = -\tfrac{1}{5} + \Pi_0\frac{2\Pi_0 + \sqrt{5+4\Pi_0^2}}{25}, \tag{7.4}$$

where $\Pi_0 = 1 + \varpi_0$. Above, the positive root of the solution has been taken which ensures that $C^a(0) = 0$, that is $F_i(R) = 0$ when $\varpi_0 = 0$.

To find the exterior solution F_e we define the auxiliary function

$$h(R) \equiv \sqrt{1+4\frac{F_e'(R)}{R}}. \tag{7.5}$$

in terms of which (7.2) simplifies to the separable equation

$$\frac{\mathrm{d}h}{\mathrm{d}R} = \frac{-5h^2+4h+1}{2h}\frac{1}{R} = f_1(h)f_2(R), \tag{7.6}$$

which can be integrated

$$\int \frac{2h}{-5h^2+4h+1}\,\mathrm{d}h = \int \frac{\mathrm{d}R}{R}. \tag{7.7}$$

The roots of $f_1(h) = 0$ are $\{h_1, h_2\} = \{-1/5, 1\}$, and cause no singularity problems since $h > 0$ and we expect $F_e' \neq 0$. The first integral above can be simplified to

$$-\frac{1}{5}\ln(5h^2-4h-1) - \frac{4}{5^2}\int \frac{\mathrm{d}h}{(h-h_1)(h-h_2)}. \tag{7.8}$$

Using the integral rule,

$$\int \frac{\mathrm{d}x}{ax^2+bx+c} = \frac{1}{\sqrt{b^2-4ac}}\ln\left(\frac{2ax+b-\sqrt{b^2-4ac}}{2ax+b+\sqrt{b^2-4ac}}\right), \tag{7.9}$$

(7.6) can be fully integrated yielding the algebraic equation

$$(h+1/5)(h-1)^5 = (R_1/R)^{15}. \tag{7.10}$$

In terms of $Y(R) \equiv h(R) - 1 = 4F_e'(R)/R$, the sextic equation (7.10) can be rewritten as

$$Y^6 + \tfrac{6}{5}Y^5 = \left(\frac{R_1}{R}\right)^{15}. \tag{7.11}$$

The integration constant R_1 can be obtained by imposing the continuity of F at $R = R_0$, that is, $F_i'(R_0) = F_e'(R_0)$, which implies that

$$\sqrt{1+4\frac{F_i'(R_0)}{R_0}} = \sqrt{1+4C^a} = \sqrt{1+4\frac{F_e'(R_0)}{R_0}} = h(R_0), \tag{7.12}$$

https://doi.org/10.1017/S0022112008003364 Published online by Cambridge University Press

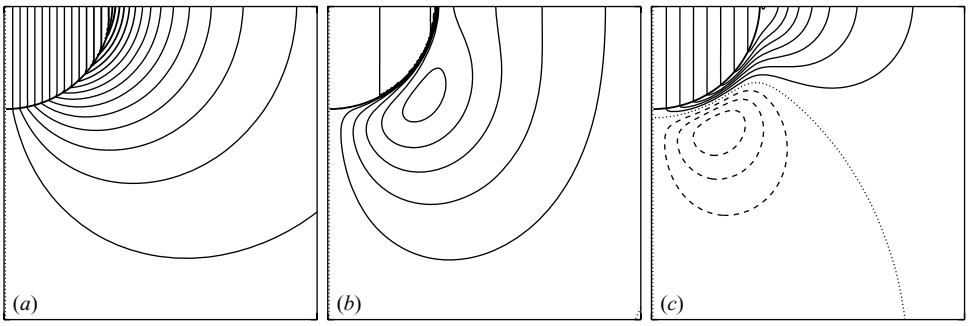


FIGURE 11. Vertical distributions of (*a*) $\tilde{v}^a$ as defined by (7.14*a*) with $\varpi_0 = 0.5$ and $R_0 = 0.5$ ($\Delta = 5 \times 10^{-2}$), (*b*) $\tilde{v} - \tilde{v}^a$ as defined by (7.14*a*) ($\Delta = 10^{-2}$), and (*c*) $\tilde{v} - \tilde{v}^s$ with $\varpi_0 = 0.5$ and $\tilde{v}^s$ computed from (6.25) and (6.3) ($\Delta = 5 \times 10^{-4}$).

and therefore from (7.10) we finally obtain R_1 as a function of ϖ_0 and R_0,

$$R_1(\varpi_0, R_0) = (\sqrt{1 + 4C^a(\varpi_0)} + 1/5)^{1/15}(\sqrt{1 + 4C^a(\varpi_0)} - 1)^{1/3} R_0. \tag{7.13}$$

We note that the exterior solution depends on the interior solution through the coefficient C^a. Alternatively, we may use the exact solution Φ_i (4.13) for the vortex interior, and the approximate solution Φ_e^a for the vortex exterior. In this case C^a in (7.13) must be replaced with C given by (4.16).

Unfortunately, the sextic equation (7.11) cannot be solved in radicals for every value of R, though it can be solved for special values of R (e.g. Head 1979). However, Y depends only on R and therefore numerical solution of (7.11) is easier than the two-dimensional equation (4.6) for $\Phi(r, \hat{z})$. Once $Y(R)$ is known it is necessary to define the velocity $\tilde{v}^a$ and $\mathscr{D}^a$ in terms of Φ^a. A simple way of doing this is to use the same relations in terms of Φ (4.3),

$$\tilde{v}^a \equiv \frac{r}{2}\left(\sqrt{1 + 4\frac{\Phi_r^a}{r}}\right) = \frac{h-1}{2} r = \frac{Y}{2} r, \quad \mathscr{D}^a \equiv -\epsilon^2 \Phi_z^a = -\frac{\epsilon(Y+2)Y}{4}\hat{z}. \tag{7.14a, b}$$

so that $Y(r)/2$ can be interpreted as the angular velocity of the fluid particle in the vortical flow. The velocity $\tilde{v}^a$, obtained from the numerical solution of (7.11) with $C^a \to C$, is shown in figure 11(*a*). The comparison with the exact v (obtained from the numerical solution of Φ) shows typical differences of one order of magnitude smaller than $|v|$ (figure 11*b*). The difference $v - v^s$, where v^s is the non-radial numerical solution for $\varpi^s(R > R_0) = 0.5$ (figure 11*c*), is smaller, typically two orders of magnitude smaller than $|v|$.

7.2. *Linear approximation*

In this approximation, the square root in (7.1) is linearly approximated using the first two terms in the Taylor series

$$\sqrt{1 + 4\frac{\Phi_r}{r}} \cong 1 + 2\frac{\Phi_r}{r}. \tag{7.15}$$

This leads to the radial equation for $\Phi^l(r, \hat{z}) = F(R(r, \hat{z}))$

$$F'' + 2\frac{F'}{R}(1 - \varpi_0) = \varpi_0, \tag{7.16}$$

https://doi.org/10.1017/S0022112008003364 Published online by Cambridge University Press

which has the interior solution

$$\Phi_i^l(R) = \tfrac{1}{2}C^l R^2, \quad C^l(\varpi_0) = \frac{\varpi_0}{3 - 2\varpi_0}. \tag{7.17a, b}$$

The exterior equation (with $\varpi_0 = 0$) is identical to the exterior QG equation ((5.8*c*) with $\varpi_I^q = 0$). Integration of this equation, and imposing continuity of F' at $R = R_0$ to obtain the integration constant, yields the exterior solution

$$\Phi_e^{l\prime}(R) = C^* \frac{R_0^3}{R^2}, \tag{7.18}$$

where C^* is either the exact C, (4.16), or the linear C^l, (7.17*b*). The external linear solution for $\Phi_e^{l\prime}$ has therefore the same R^{-2} dependence as the QG solution $\Phi_e^{q\prime}$, (5.11*b*).

7.3. *Upper and lower bound solutions*

On rewriting the exact PV equation (4.12) as

$$\Pi_0\sqrt{1 + 4\frac{F'}{R}} = F'' + \left(1 + 2\frac{F'}{R}\right)^2 + \frac{F'}{R}\left(F'' - \frac{F'}{R}\right)\frac{R^2 + 3\hat{z}^2}{R^2}, \tag{7.19}$$

approximate radial solutions can be found solving special cases of the family of equations

$$\Pi_0\sqrt{1 + 4\frac{F'}{R}} = F'' + \left(1 + 2\frac{F'}{R}\right)^2 + \frac{F'}{R}\left(F'' - \frac{F'}{R}\right)\frac{T_\gamma(r, \hat{z})}{R^2}. \tag{7.20}$$

Above

$$T_\gamma(r, \hat{z}) \equiv R^2 + 3\hat{z}^2 + \gamma\tfrac{3}{2}\left\{R^2 + \gamma(r^2 - \hat{z}^2)\right\}, \tag{7.21}$$

so that with $T_0(r, \hat{z}) = R^2 + 3\hat{z}^2$ we recover (7.19), while $T_{-1}(r, \hat{z}) = R^2$ and $T_{+1} = 4R^2$ are radial terms such that $T_{-1} \leqslant T_0 \leqslant T_1$. Thus, (7.20) admits radial solutions for $\gamma = \{-1, 1\}$. As in the previous section, we define $h^2 \equiv 1 + 4F'/R$. As occurs with (7.2), the differential equation (7.20) can be analytically integrated, but the solution h cannot be analytically expressed as a function of R. The integration of (7.20) for $\gamma = -1$ and $\gamma = +1$ (Appendix) leads, respectively, to

$$\frac{R_-(h)}{R_-^0} = f_-(h) = \frac{\exp\left\{\frac{1}{2\sqrt{15}}\arctan\left(\frac{2h+1}{\sqrt{15}}\right)\right\}}{(h-1)^{1/3}(h^2 + h + 4)^{1/12}}, \tag{7.22a}$$

$$\frac{R_+(h)}{R_+^0} = f_+(h) = \frac{\exp\left\{-\frac{1}{\sqrt{15}}\arctan\left(\frac{2h+1}{\sqrt{15}}\right)\right\}}{(h-1)^{1/3}(h^2 + h + 4)^{5/6}}, \tag{7.22b}$$

where the constants $R_\pm^0$ are obtained imposing continuity of h at $R = 0$,

$$R_\pm^0 = \frac{R_0}{f_\pm(h_0)}, \quad h_0 = \sqrt{1 + 4C}. \tag{7.23}$$

We note that the interior solution F_i satisfies $F'' = F/R$ so that the last term in (7.20) is zero, and F_i is unique, independent of T_γ. The radial solutions (7.22), plotted as functions of $(h^2 - 1)/4 = F'/R$ in figure 12(*a*), are lower and upper bounds to the numerical solution $\Phi_r(r, \hat{z})/r$ of the exact equation (4.6). The lower bound R_- is very similar to the linear solution $\Phi^{l\prime}/R$ (figure 12*a*).

https://doi.org/10.1017/S0022112008003364 Published online by Cambridge University Press

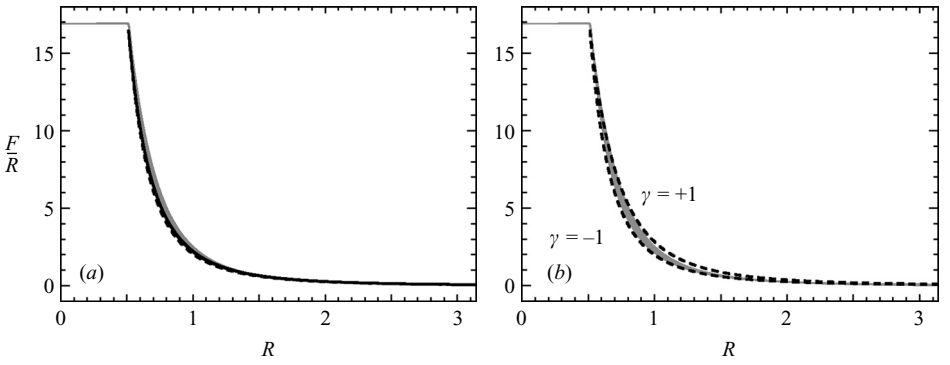


FIGURE 12. (*a*) Solution $\Phi^a(R)/R$ ($\times 10^2$, dashed line) as deduced from (7.10), and linear solution $\Phi^l(R)/R$ ($\times 10^2$, continuous line) given by (7.18). (*b*) Solutions R_- and R_+ and in the horizontal axis) given by (7.22) but as a function of $F'/R = (h^2 - 1)/4$ ($\times 10^2$, vertical axis). In (*a*) and (*b*), the boundary condition for the different F'/R at $R = R_0$ is that corresponding to the exact interior solution, thus in fact using $C^a \to C$ and $C^l \to C$. The scatterplot of the numerical solution $\Phi_r(r, \hat{z})/r$ of the exact equation (4.6) versus R (as in figure 5) is included in both figures for comparison.

8. Concluding remarks

In this paper, we have explored the concept of piecewise constant symmetric finite-size PV vortices as a possible alternative to point vortices in inertially and statically stable geophysical flows. Solutions, either analytical or numerical, for the pressure gradient as a function of the PV anomaly, or the respective material invariant, and radius of the PV ball have been found. An exact analytical solution for the non-radial pressure gradient in the vortex exterior in the case of the full (Boussinesq and f-plane approximations) dynamics remains, however, as an important theoretical challenge. These PV ball vortices may be particularly useful in numerical simulations where it can be assumed that the velocity shear is numerically meaningless at the small subgrid scales. Under these circumstances it may be justified that the PV balls with a radius much smaller than the grid size are simply advected, but not deformed, by the background flow, so that the PV balls remain always spherical. These PV balls will not cause static or inertial instabilities even when a numerical grid point is located inside the PV sphere. Investigation along this numerical research line is the next step.

I am grateful to T. Piezas for his help on the sextic equation (7.11).

Appendix. Integration of (7.22)

For $\gamma = -1$ and $h^2 \equiv 1 + 4F'/R$, (7.22) reduces to the separable equation

$$8 - 2h(h^2 + 3) = (h^2 + 3)h'R, \tag{A 1}$$

which can be integrated

$$-\frac{1}{2}\int \frac{h^2 + 3}{h^3 + 3h - 4}\,\mathrm{d}h = \int \frac{\mathrm{d}R}{R}. \tag{A 2}$$

https://doi.org/10.1017/S0022112008003364 Published online by Cambridge University Press

The integral on the left-hand side is

$$-\tfrac{1}{2}\int \frac{h^2+3}{h^3+3h-4}\,\mathrm{d}h = -\tfrac{1}{6}\ln(h^3+3h-4) - \int \frac{\mathrm{d}h}{h^3+3h-4}. \tag{A 3}$$

To integrate the last term we factorize $h^3+3h-4=(h-1)(h^2+h+4)$, and noticing that the roots of $h^2+h+4=0$ are complex we use the integral rule

$$\int \frac{\mathrm{d}x}{ax^2+bx+c} = \frac{2}{\sqrt{4ac-b^2}}\arctan\left(\frac{2ax+b}{\sqrt{4ac-b^2}}\right), \tag{A 4}$$

which yields

$$\int \frac{\mathrm{d}h}{h^3+3h-4} = \ln\left[\frac{(h-1)^{1/6}}{(h^2+h+4)^{1/12}}\right] - \frac{1}{2\sqrt{15}}\arctan\left(\frac{2h-1}{\sqrt{15}}\right). \tag{A 5}$$

Case $\gamma=1$ is solved in a similar way.

REFERENCES

Batchelor, G. K. 1967 *An Introduction to Fluid Dynamics*. Cambridge University Press.

Beltrami, E. 1871 Sui principii fondamentali dell'idrodinamica razionali. *Memorie della Accademia delle Scienze dell'Instituto di Bologna* **1**, 431–476.

Charney, J. G. 1971 Geostrophic turbulence. *J. Atmos. Sci.* **28**, 1087–1095.

Dritschel, D. G. & Viúdez, A. 2003 A balanced approach to modelling rotating stablystratified geophysical flows. *J. Fluid Mech.* **488**, 123–150.

Eliassen, A. 1949 The quasi-static equations of motion with pressure as independent variable. *Geofys. Publ.* **17**(3), 1–44.

Ertel, H. 1942 Ein neuer hydrodynamischer erhaltungssatz. *Naturwissenschaften* **30**, 543–544.

Fjortoft, R. 1962 On the integration of a system of geostrophically balanced prognostic equations. In *Proc. Intl Symp. Numerical Weather Prediction*. Met. Soc. Japan, Tokyo.

Head, A. K. 1979 The monodromic Galois groups of the sextic equation of anisotropic elasticity. *J. Elasticity* **9**, 321–324.

Holton, J. R. 2004 *An Introduction to Dynamic Meteorology*. Elsevier.

Hoskins, B. J. 1975 The geostrophic momentum approximation and the semi-geostrophic equations. *J. Atmos. Sci.* **32**, 233–242.

Hoskins, B. J. & Draghici, I. 1977 The forcing of ageostrophic motion according to the semi-geostrophic equations and in an isentropic coordinate model. *J. Atmos. Sci.* **34**, 1859–1867.

Kurgansky, M. V. & Tatarskaya, M. S. 1987 The potential vorticity concept in meteorology: a review. *Izv. Atmos. Ocean. Phys.* **23**, 587–606.

Lamb, H. 1932 *Hydrodynamics*. Cambridge University Press.

Müller, P. 1995 Ertel's potential vorticity theorem in physical oceanography. *Rev. Geophys.* **33**, 67–97.

Nolan, D. S. & Montgomery M. T. 2002 Nonhydrostatic, three-dimensional perturbations to balanced, hurricane-like vortices. Part I: Linearized formulation, stability, and evolution. *J. Atmos. Sci.* **59**, 2989–3020.

Rossby, C.-G. 1940 Planetary flow patterns in the atmosphere. *Q. J. R. Met. Soc.* **66** (suppl.), 68–87.

Saffman, P. G. 1992 *Vortex Dynamics*. Cambridge University Press.

Shutts, G. J. 1991 Some exact solutions to the semi-geostrophic equations for uniform potential vorticity flows. *Geophys. Astrophys. Fluid Dyn.* **57**, 99–114.

Thorpe, A. J. & Bishop, C. H. 1994 Potential vorticity and the electrostatics analogy – quasi-geostrophic theory. *Quart. J. Roy. Met. Soc.* **120**, 713–731.

Thorpe, A. J. & Bishop, C. H. 1995 Potential vorticity and the electrostatics analogy – Ertel–Rossby formulation. *Q. J. R. Met. Soc.* **121**, 1477–1495.

Viúdez, A. 2001 The relation between Beltrami's material vorticity and Rossby–Ertel's potential vorticity. *J. Atmos. Sci.* **58**, 2509–2517.

https://doi.org/10.1017/S0022112008003364 Published online by Cambridge University Press

Viúdez, A. 2005 The vorticity–velocity gradient cofactor tensor and the material invariant of the semigeostrophic theory. *J. Atmos. Sci.* **62**, 2294–2301.

Viúdez, A. & Dritschel, D. G. 2003 Vertical velocity in mesoscale geophysical flows. *J. Fluid Mech.* **483**, 199–223.

Voropayev, S. I. & Afanasyev, Y. D. 1994 *Vortex Structures in a Stratified Fluid. Order from Chaos*. Chapman & Hall.

White, A. A. 2002 A view of the equations of meteorological dynamics and various approximations. In *Large-Scale Atmosphere-Ocean Dynamics I* (ed. J. Norbury & I. Roulstone), pp. 1–100. Cambridge University Press.

https://doi.org/10.1017/S0022112008003364 Published online by Cambridge University Press